

Optimizing Statistical Methods for Connectivity Mapping in MR Neuroimaging

By

Anita Meghan Sinha

A dissertation submitted in partial fulfillment of
the requirements for the degree of

Doctor of Philosophy
(Biomedical Engineering)

at the

UNIVERSITY OF WISCONSIN-MADISON

2021

Date of final oral examination: 07/20/2021

The dissertation is approved by the following members of the Final Oral Committee:

Mary Elizabeth Meyerand, Professor, Biomedical Engineering

Vivek Prabhakaran, Associate Professor, Radiology

Walter Block, Professor, Biomedical Engineering

Rasmus Birn, Associate Professor, Medical Physics

Vikas Singh, Professor, Biostatistics & Medical Informatics

Acknowledgements

This dissertation is the culmination of many years of work and represents the capstone of a graduate education that was forged at the University of Wisconsin-Madison. There are many individuals to whom I owe immense thanks for their mentorship and support during my time here, as this work would not have been possible without them.

To my advisor, Dr. Vivek Prabhakaran: thank you for the opportunity to pursue a Ph.D. under your supervision. Your guidance and wisdom, along with allowing me the autonomy to pursue projects and professional opportunities that were fun, challenging or simply piqued my interest, have been critical to my graduate education experience and growth as a research scientist and engineer. To my Biomedical Engineering advisor, Dr. Mary Elizabeth Meyerand: thank you for your mentorship throughout my journey in graduate school. It has played an instrumental role in helping me set and achieve my goals and prepared me to tackle future endeavors with confidence and enthusiasm.

To the rest of my committee members, Dr. Walter Block, Dr. Rasmus Birn and Dr. Vikas Singh: it has been an absolute pleasure working with you all. Your combined experience and expertise in the field have been crucial to the progress and quality of my work. Thank you for teaching me to approach science with curiosity, rigor, respect and patience, as it has inspired me to continually strive to be the best scientist I can be.

To our research scientist in the Prabhakaran lab, Dr. Veena Nair: thank you for your patience, kindness and expertise in the field. You always made time in your busy schedule

to talk regularly with me about any aspect of research, and our insightful discussions played a key role in the quality and success of the work presented here. I consider it a privilege and honor to have learned from and worked alongside you.

To my fellow lab members in the Prabhakaran lab, notably Rosaleena Mohanty, Keith Dodd, Cole Cook and Gyujoon Hwang: thank you for always being there to bounce ideas off of and for your willingness and excitement to question and talk through the most minute of details related to our research. To Ronak Mehta, a graduate student under Dr. Vikas Singh: thank you for your patience, expertise in computer science and statistics and the years of collaboration and enthusiasm for our work together.

To Mallory and Adam Klinger whom I have known since my first year of undergrad at Wisconsin: thank you for our friendship and for being best friends who feel like family. Thank you for always having me over to visit in Chicago and Oshkosh and for all of the fun times exploring the city, summer/winter hiking, wakeboarding, kayaking, ice skating and many more. To my best friend from undergrad, Doug Fraser: although we live in different regions and time zones of the country, the distance never seemed that far with our weekly phone and Zoom calls that were always filled with hours of laughter. I'm glad we could share our graduate school experiences together. To my other fellow Badger friends, Sarah Swanson, Kaley Zanghi, Bahar Behzadnezhad and Britney Washington: thank you for making my time at Wisconsin such an enjoyable experience.

To my parents, Atul and Binita Sinha: thank you for the endless and immeasurable love and support as my biggest cheerleaders through every interest and passion I have ever pursued. Growing up in a home that fosters a love of learning and watching everything you both have accomplished together have been my greatest inspirations to continually seek out and pursue new opportunities and experiences with eagerness and curiosity. And through it all, thank you Mom and Dad for never explicitly telling me how to navigate life, but instead providing me with the tools and wisdom to do so with confidence, open-mindedness and humility. To my sister, Natasha: although our 7 year age difference means we go

through stages of life at different times, you never cease to amaze me with your wisdom and perspectives on life. Thank you for always reminding me to appreciate the present.

Abstract

Magnetic resonance imaging (MRI) plays an integral role in the study, diagnosis and treatment of neurological diseases. Neuroimaging analyses involve high-dimensional, large-scale data that contain rich spatial and temporal information about the dynamic and integrated systems in the brain. Therefore, it has become increasingly imperative to develop and optimize analytical approaches drawn from engineering and mathematics to more precisely model these complex patterns and interactions, which will advance our understanding of functional brain organization in health and disease.

Chapter 1 provides an overview and background of MRI, with a particular focus on the use of resting-state functional magnetic resonance imaging (rs-fMRI) to capture and characterize brain connectivity. Previous work of statistical methods developed and widely used for analysis of fMRI are reviewed.

Chapter 2 presents an analysis of changes in functional connectivity and behavioral outcomes in patients of stroke who undergo brain-computer interface (BCI) interventional therapy. This work employs a widely used network-based inference method for fMRI analysis that serves as motivation for subsequent work to overcome statistical challenges associated with its use to more effectively model and characterize brain network dynamics and organization in a robust manner.

Chapter 3 presents a novel application of differential covariance trajectory analysis as promising framework for brain network modeling using rs-fMRI data. The proposed algo-

rithm models functional connectivity as trajectories on the manifold and employs a localization procedure to efficiently search over and identify subsets of first- and second-order differences in brain connectivity features between patients with Temporal Lobe Epilepsy (TLE) and healthy control subjects.

Chapter 4 extends the work presented in the previous chapter to apply the combined differential covariance trajectory and scan statistics framework to characterize the Alzheimer's Disease (AD) connectome. We demonstrate the utility and robustness of this method to study altered brain network organization in large-scale functional networks in a different and older clinical population, which is notably of smaller sample size, where the statistical signal may be weak.

Chapter 5 discusses conclusions and key takeaways of the work, along with potential future avenues of research.

Contents

1	Introduction and Background	1
1.1	Functional Magnetic Resonance Imaging	2
1.2	Traditional analysis methods for fMRI	3
1.2.1	Static functional connectivity	3
1.2.2	Dynamic functional connectivity	5
1.3	Manifold learning	6
1.3.1	Riemannian geometry preliminaries	6
1.3.2	Manifold-based methods for fMRI analysis	8
1.4	Motivation	9
2	Determining the effects of BCI therapy with FES on chronic stroke patients using traditional statistical methods for functional connectivity analysis	12
2.1	Introduction	13
2.1.1	Overview of study	15
2.2	Materials and methods	16
2.2.1	Participants	16
2.2.2	Study design	18
2.2.3	BCI intervention	18
2.2.4	Data acquisition: neuroimaging	21
2.2.5	Data acquisition: behavioral outcome measures	22

	vii
2.2.6	Data preprocessing 22
2.2.7	Functional connectivity analysis 23
2.2.8	Group-level analysis 24
2.3	Results 25
2.3.1	Functional connectivity in the motor network 25
2.3.2	Behavioral outcome analysis 27
2.3.3	Associations between changes in functional connectivity and behav- ioral outcome measures 28
2.4	Discussion 30
2.4.1	Functional connectivity changes associated with intervention 31
2.4.2	Improvements in behavioral outcomes associated with intervention 32
2.4.3	Relationship between changes in functional connectivity and functional outcomes 33
2.4.4	Limitations 35
2.5	Conclusions 36
3	Characterizing the Epilepsy Connectome via Differential Covariance Anal- ysis, a new mathematical network-based inference framework for modeling functional connectivity 37
3.1	Introduction 38
3.2	Methods 42
3.2.1	Scan statistics and an alternative testing correction 42
3.2.2	Likelihood Ratio Statistics 45
3.2.3	Estimating μ_t, Σ_t via Regression 46
3.2.4	Trajectories on high-dimensional covariance matrices 48

3.3	Experiments	50
3.3.1	Data and preprocessing	50
3.3.2	Baseline comparison methods	52
3.3.3	Experimental setup	53
3.3.4	Altered connectivity findings from baseline experiments	55
3.3.5	Networks identified using covariance trajectory analysis	57
3.4	Discussion and Conclusion	58
4	Characterizing the Alzheimer’s Disease Connectome via Differential Co- variance Analysis	60
4.1	Introduction	61
4.2	Methods	62
4.2.1	Scan statistics: a multiple testing procedure	62
4.2.2	Modeling covariance trajectories	63
4.2.3	Data and Experiments	64
4.3	Results	66
4.3.1	Altered connectivity findings from baseline experiments	66
4.3.2	Altered functional brain networks identified using new pipeline	67
4.4	Discussion and conclusion	68
5	Summary and Future Work	70
5.0.1	Summary	71
5.0.2	Future work	72

List of Figures

1.1	The general frameworks for sFC and dFC analyses. (a) Illustration of the sFC method. Each (i, j) element is the Pearson correlation coefficient between the timeseries of the i th and j th ROI over the full fMRI scan. (b) Illustration of the basic sliding window method. Correlation matrices are calculated across successive, overlapping windows in the timeseries to capture the dFC profile across brain regions and networks. Often times, a temporal variability matrix is computed, where each (i, j) element is a summary measure of variation in connectivity across temporal windows.	4
1.2	Illustration of the difference between the Euclidean distance (blue) and geodesic distance (orange) between two points X and Y on the SPD manifold.	7
1.3	Projection of a point in the tangent space to the manifold \mathcal{M} via the exponential map.	8
2.1	Study schedule for BCI intervention.	18
2.2	Electrode placement in 16-channel EEG cap used in BCI system (red – active electrodes, yellow – ground electrode, blue – reference site on right ear lobe) adapted from (Remsik et al., 2019). Signals from electrode channels C3 and C4 served as input into the BCI classifier to control lateral cursor movement.	19

2.3	From pre-intervention to post-intervention, significant correlations were identified between changes in (A) SIS ADL and interhemispheric connectivity, (B) SIS Mobility and interhemispheric connectivity and (C) SIS ADL and average network connectivity. (D) From pre-intervention to one month post-intervention, changes in ARAT negatively correlated with interhemispheric connectivity changes.	28
3.1	Overview of the proposed framework. The full procedure involves: (1) pre-processing fMRI data, (2) extracting timeseries from ROIs in parcellation, (3) computing subject-specific covariance matrices across time windows, (4) selecting subset of features from the input graph, (5) fitting linear and manifold regression of covariances for both groups (G_1 and G_2) and (6) computing likelihood ratio statistic and comparing against null distribution via permutation testing.	41
3.2	In graph scan statistics, a search procedure is iteratively performed across various subsets of features in the input graph to compute the between-group difference for each subset and obtain the local statistic.	43
3.3	(a) 360 ROIs from the surface-based parcellation Glasser et al. (2016). (b) Graphical representation of the input graph of the parcels in their respective network.	50
3.4	Results from baseline scan statistics method with the corresponding estimated null distribution and alternative statistic. (Left) Posterior Cingulate Cortex, (Right) Medial Temporal Cortex. B - visualization from back.	56

3.5	Networks exhibiting significant first- and second-order group differences using the proposed method with the corresponding estimated null distribution and alternative statistic: (from left to right) Subcortical, Insular and Frontal Opercular Cortex, Inferior Frontal Cortex, Orbital and Polar Frontal Cortex. S - saggital view, R - visualization from the right, F - visualization from the front.	58
4.1	The pipeline involves: (1) selecting a subset of features, (2) fitting manifold regressions on empirical covariances for both groups (green and purple) and (3) constructing the likelihood ratio statistic and comparing it against the null distribution via permutation testing.	62
4.2	360 parcels in their respective functional brain network based on Ji et al. (2019).	65
4.3	Functional networks exhibiting significant first- and second-order group differences with the corresponding estimated null distribution and alternative statistic (red) using our pipeline (brain visualization from right).	68

List of Tables

2.1	Demographic information of subjects.	17
2.2	Significant interhemispheric and intrahemispheric connections at each time point identified using NBS (Zalesky et al. 2010) based on t-statistic ($p <$ 0.05).	26
2.3	GEE analysis of behavioral outcome measures.* $0.05 < p < 0.1$	27
2.4	Correlations between change in average and interhemispheric rsFC and be- havior. * $0.05 < p < 0.1$	29
3.1	Brain networks from Glasser et al. (2016) and FreeSurfer subcortical network	50
3.2	Demographic information of subjects.	51
3.3	Networks exhibiting significant group differences from the baseline sFC and dFC methods.	55
4.1	Networks exhibiting significant group differences from sFC and dFC analyses.	67

Chapter 1

Introduction and Background

1.1 Functional Magnetic Resonance Imaging

Magnetic resonance imaging (MRI) is a non-invasive imaging modality that employs strong magnetic fields in combination with radiofrequency waves to construct detailed three-dimensional anatomical images. Specifically, MRI uses signals generated from proton dynamics in the magnetic field to measure water content in different regions of the body, producing images with rich soft tissue contrast resolution. Many diseases in soft tissues such as the brain manifest as markedly increased water content either regionally or globally that result in functional and structural abnormalities. Given these properties, the high resolution and multiplanar capabilities MRI offers has made it a primary imaging modality in both the clinic and research settings for diagnosis and treatment monitoring of neurological diseases.

Functional magnetic resonance imaging (fMRI) has revolutionized the fields of radiology and neuroscience research by enabling us to capture time-varying changes in cerebral metabolism to study brain function. During sensory or cognitive processes, neuronal activation elicits an increase in regional cerebral blood flow due to elevated metabolic activity and results in an increased demand in oxygenated blood (Menon and Kim, 1999). Oxygenated hemoglobin is diamagnetic and deoxygenated hemoglobin is paramagnetic, and fMRI leverages these differences in magnetic properties in the blood to generate what is known as the blood oxygenation level-dependent (BOLD) signal in MRI. Based on changes in blood-oxygen levels, we can use fMRI to indirectly measure and infer neural activity in a non-invasive manner to study the brain's functional architecture.

In particular, resting-state functional magnetic resonance imaging (rs-fMRI) has become a ubiquitous and powerful neuroimaging tool to probe and characterize brain connectivity dynamics and their relationships to health and disease (Lee et al., 2013; Smitha et al., 2017). Resting-state functional connectivity (rsFC), extracted from rs-fMRI, measures temporal correlations between fluctuations in the spontaneous, low-frequency (0.01 – 0.1 Hz) BOLD signal across spatially distributed, but functionally connected brain regions in the absence

of an explicit task. Notably, the seminal work of Biswal et al. (1995) demonstrated an established correspondence between neuronal activation patterns at rest and those elicited in task settings across functional brain networks. These initial findings have been corroborated by hundreds of subsequent studies, including Calhoun et al. (2008); Laird et al. (2011); Smith et al. (2009), and enabled the development of various parcellation atlases that use functional connectivity patterns to characterize and map the entire brain (Gordon et al., 2016; Ji et al., 2019; Yeo et al., 2011). In addition, these works have supported the continued progress and use of advanced rs-fMRI techniques and tools that can partly circumvent challenges with task-fMRI studies and further our understanding of brain dynamics. The burgeoning field of rs-fMRI continues to garner significant attention across multiple disciplines, including but not limited to engineering, statistics and signal processing, and has resulted in a wide array of analytical methods and tools to interrogate the complexities of intrinsic brain activity and glean unique insights into functional network organization in health and disease.

1.2 Traditional analysis methods for fMRI

1.2.1 Static functional connectivity

In standard fMRI analyses, timeseries data are either extracted from P *a priori* regions of interest (ROIs) from a brain atlas or decomposed into multiple networks using independent component analysis (ICA). Then, a similarity metric, most often correlation, is calculated between the timeseries of all pairs of ROIs or components over a full scan to generate a subject-specific $P \times P$ correlation matrix as shown in Figure 1.1a. This approach of time-averaged connectivity, or popularly known as static functional connectivity (sFC), previously served as the basis for brain network modeling and afforded valuable insight into understanding brain function and aberrant connectivity in disease at the macroscale level. There is, however, substantial and increasing evidence that fluctuations in rsFC span several temporal and spatial scales (Allen et al., 2014; Hutchison et al., 2013; Preti et al., 2017; Xu et al.,

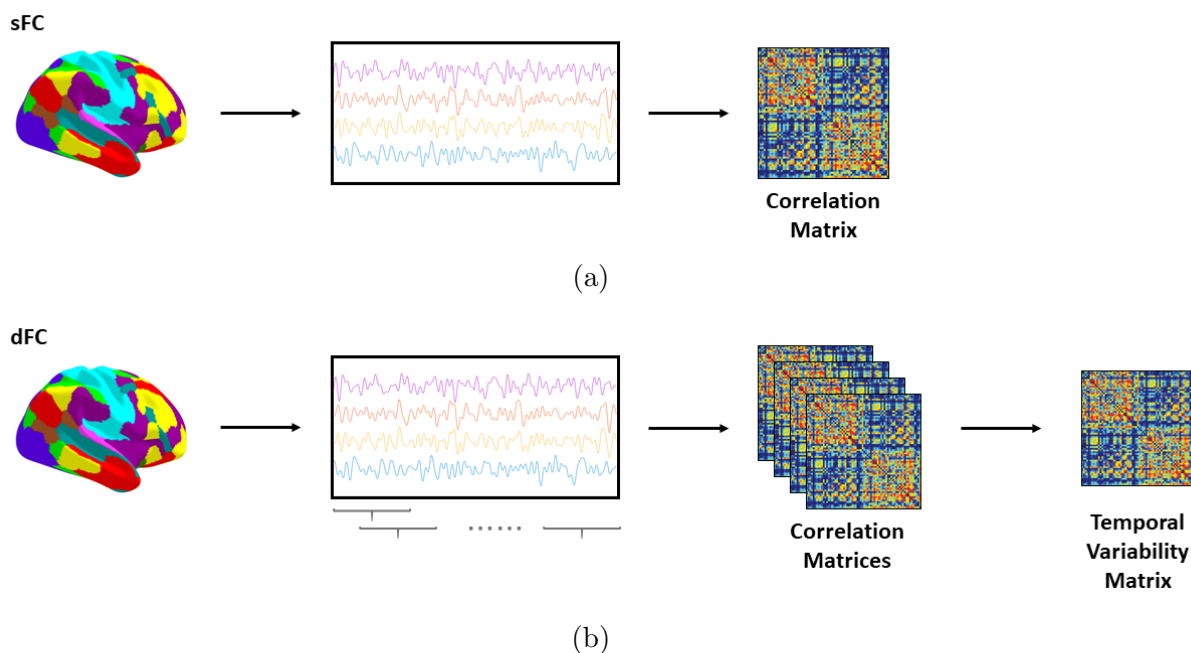


Figure 1.1: The general frameworks for sFC and dFC analyses. (a) Illustration of the sFC method. Each (i, j) element is the Pearson correlation coefficient between the timeseries of the i th and j th ROI over the full fMRI scan. (b) Illustration of the basic sliding window method. Correlation matrices are calculated across successive, overlapping windows in the timeseries to capture the dFC profile across brain regions and networks. Often times, a temporal variability matrix is computed, where each (i, j) element is a summary measure of variation in connectivity across temporal windows.

2021), challenging the implicit assumption of temporal stationarity in brain connectivity. These and a growing number of similar works argue that, while sFC provides a convenient framework for characterizing functional connectivity, it oversimplifies the nature of brain network dynamics. The brain is comprised of a complex interplay of dynamic functional interactions within and across networks that evolve over time, which is critical for normal function. Therefore, sFC may be providing a limited view of brain connectivity that does not capture the underlying spatiotemporal dynamics that are involved in the mechanisms and manifestations of disease across clinical populations.

1.2.2 Dynamic functional connectivity

Accordingly, there has been a significant shift toward developing dynamic functional connectivity (dFC) methods to more precisely capture the spatiotemporal dynamics in rsFC. The most widely used framework for modeling dFC is sliding window analysis. In its simplest form, the sliding window method involves: (1) defining a window of fixed length W , (2) computing the correlation between the timeseries of all pairs of brain regions or derived components from $t = t_i$ to $t = W$, (3) shifting the window by a pre-defined stride S and recomputing correlation and (4) iteratively repeating the procedure for each successive time window over the full timeseries as shown in Figure 1.1b. At the subject-level, this results in a correlation, or connectivity, matrix for each time window $w \in \{1 \dots \mathcal{W}\}$, where $\mathcal{W} = \frac{\text{Total TRs} - W}{S} + 1$. In conventional dFC studies, metrics such as standard deviation, coefficient of variation or variance are then computed element-wise across all correlation matrices (Hutchison et al., 2013), yielding subject-specific $P \times P$ dFC (temporal variability) matrices for group-level analyses.

More recently, there has been growing adoption of the “chronnectome” view of functional brain organization (Calhoun et al., 2014) to model the dynamically evolving spatial and temporal coupling among brain regions. Using a brain atlas or data-driven parcellation, the sliding window technique has been combined with clustering approaches such as k -means clustering (Allen et al., 2014; Menon and Kim, 1999; Shakil et al., 2016), temporal ICA (Smith et al., 2012) and dictionary learning (Li et al., 2014) to identify transient dFC patterns or “brain states”. The conceptual framework of sliding window analysis has also been used to develop dFC change point detection algorithms at both the subject- and group-level (Betz et al., 2016; Cribben et al., 2012, 2013; Xu and Lindquist, 2015). Alternative approaches employ time-frequency analysis (Chang and Glover, 2010; Omidvarnia et al., 2016; Yaesoubi et al., 2015) and window-less methods (Yaesoubi et al., 2018) to analyze the time-varying patterns and dFC states. Leveraging the natural representation of brain

networks in graphical form, other techniques have used graph theory (Chiang et al., 2016), community detection methods (Betzel et al., 2016) and temporal graphical models (Schwab et al., 2018) to characterize the topological organization and dynamics of brain networks. For a systematic and full review of methodological frameworks and techniques for modeling dFC, refer to Hutchison et al. (2013); Lurie et al. (2020); Preti et al. (2017).

1.3 Manifold learning

1.3.1 Riemannian geometry preliminaries

We briefly describe some basic concepts and notations in Riemannian geometry in the context of fMRI analysis. Let \mathcal{M} be a smooth manifold, or topological space, that resembles Euclidean space locally and has a globally defined differential structure. A Riemannian manifold is a differential manifold \mathcal{M} with a smoothly varying inner product on each tangent space $T_p\mathcal{M}$. $P \times P$ covariance or correlation (normalized form of covariance) matrices are symmetric and positive definite (SPD), and the set of all SPD matrices lie on a Riemannian manifold, or positive semidefinite cone. A matrix $X \in \mathbb{R}^{P \times P}$ is symmetric if it satisfies the property $X = X^T$ and positive definite if its eigenvalues $\lambda_1, \dots, \lambda_n \geq 0$. Note that covariance matrices estimated on real-world data may not always be positive definite, therefore, we can project the estimated covariance matrix onto the SPD manifold and perform a simple regularization procedure as described in Mehta et al. (2019) when needed to resolve this. A mathematical proof of these properties in the context of functional connectivity analysis can be found in Venkatesh et al. (2020). We can leverage these geometric characteristics in SPD space and perform statistical analyses on the entire covariance matrices on the manifold.

If covariance matrices are represented on the manifold, the distance between them is no longer in Euclidean space, but instead along the surface of the cone. Accordingly, this motivates the use of mathematical operations that better align with the geometric characteristics and conditions of the SPD space. This can be conceptualized as follows: in Euclidean space,

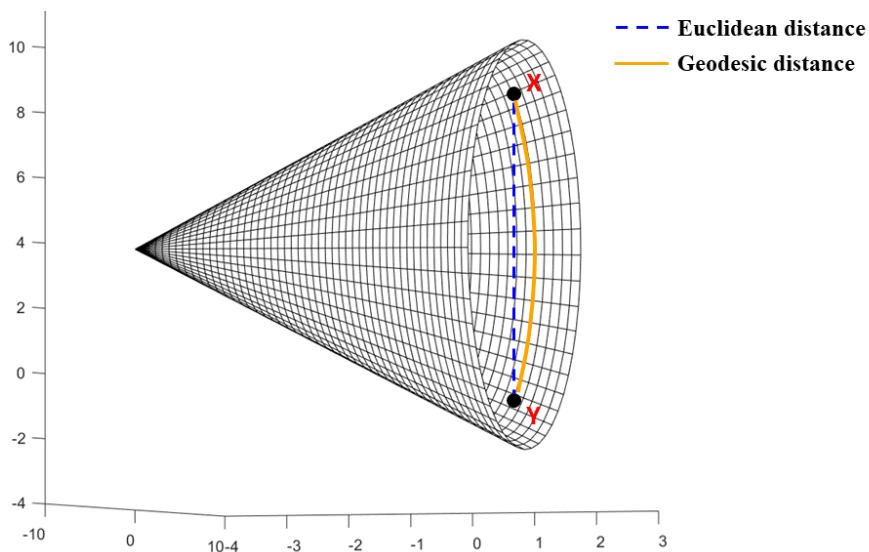


Figure 1.2: Illustration of the difference between the Euclidean distance (blue) and geodesic distance (orange) between two points X and Y on the SPD manifold.

we can simply use the Pythagorean Theorem to calculate the distance between two points. In the manifold setting, however, this computation cannot be used to represent the distance because a straight line connecting two points would go through or lie inside the manifold, thereby not respecting the geometry of SPD space. In order to find the distance between two points on the manifold, the path must lie on the manifold on which it is defined and thus must be a curve.

Generalizing the notion of straight lines in Euclidean space to the Riemannian manifold, the locally shortest (distance-minimizing) path between two points or covariance matrices X and Y is the geodesic curve. The geodesic curve can be used to define the “trajectory” of covariance matrices over time in SPD space. Unlike Euclidean space, multiple geodesic curves may exist that connect two points on \mathcal{M} . The length of the shortest geodesic curve connecting two points on a Riemannian manifold is the geodesic distance. The difference between Euclidean distance and geodesic distance on the manifold is shown in Figure 1.2. A number of Riemannian metrics have been proposed to calculate the geodesic distance on the SPD manifold, however, the two most widely used in the literature are the Affine Invariant Riemannian Metric (AIRM) (Pennec et al., 2006) and Log-Euclidean metric (LEM) (Arsigny

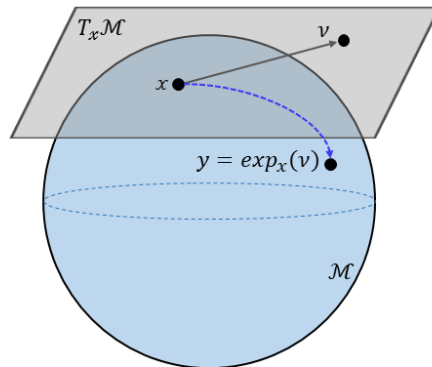


Figure 1.3: Projection of a point in the tangent space to the manifold \mathcal{M} via the exponential map.

et al., 2006).

The exponential map, $\text{Exp}(x_i, \cdot) : T_{x_i} \mathcal{M} \rightarrow \mathcal{M}$, defines a geodesic curve from x_i to x_j in the direction of the tangent vector v in the tangent space $T_x \mathcal{M}$ to a point on the manifold as shown in Figure 1.3. In other words, the exponential map is a projection from Euclidean space onto the manifold. The inverse of the exponential map is the logarithmic map, $\text{Log}(x_i, \cdot) : \mathcal{M} \rightarrow T_{x_i} \mathcal{M}$, which projects a given point on the manifold back to the tangent vector. Using these mathematical operations, we can go back and forth between the manifold space of the SPD matrices and the tangent space of covariate or predictor variables. For additional details of preliminaries on Riemannian geometry and a brief overview of algorithms on the manifold specific to fMRI analysis, see You and Park (2021). A comprehensive review of Riemannian geometry can be found in Lee (2006).

1.3.2 Manifold-based methods for fMRI analysis

In the last decade, manifold learning methods have been successful in deriving clinically meaningful representations from neuroimaging data that are not achievable with classical models (Fletcher and Joshi, 2007; Kim et al., 2014; Xie et al., 2010). In the context of fMRI, functional connectivity can be represented as symmetric positive definite (SPD) matrices that form a Riemannian manifold, enabling us to leverage the geometric properties described

above and perform statistical analyses on the manifold. Features of Riemannian metrics on the SPD manifold have been used to detect inter-subject differences in functional connectivity (Varoquaux et al., 2010) and hold predictive power for both classification and regression (Wong et al., 2018) between healthy controls and various patient cohorts. Related work have proposed using the geodesic distance to compare functional connectivity matrices for participant identification instead of the traditional Pearson correlation (Venkatesh et al., 2020) and to quantify similarity in functional brain networks (Yamin et al., 2019). Moreover, Riemannian-based frameworks have been developed to characterize longitudinal rs-fMRI trajectories (Zhao et al., 2018) and coupled with dimensionality reduction techniques for applications in machine learning (Dai et al., 2019; Ng et al., 2015; Qiu et al., 2015; Zhang et al., 2015). Although manifold-based frameworks and tools are a new and growing area within the fMRI community, these existing works have shown them to be effective methods for modeling the high-dimensional, multivariate nature of large-scale functional connectivity.

1.4 Motivation

Independent of the technique used to model functional connectivity, group-level analyses largely rely on the use of univariate hypothesis testing (e.g. t -test) with a correction for multiple comparisons, such as Bonferroni correction to control the family-wise error rate (FWER) or the Benjamini–Hochberg procedure (Benjamini and Hochberg, 1995) to control the false discovery rate (FDR). Connections that survive the significance threshold constitute discriminative features that stratify groups. In comparisons between patient and control cohorts, statistical differences in connectivity features are commonly considered biomarkers of disease. This design choice of a hypothesis testing procedure implicitly treats connections as statistically independent features, which poses several challenges in brain network analyses.

First, mass univariate analyses can often either overestimate the significance of group differences or fail to identify differential effects due to poor effect sizes. This is particularly

relevant in neuroimaging analyses, which commonly use high dimensional data from a limited sample size (typically a few hundred individuals at most). Second, interactions among groups of connections that evolve over time, which are inherent in functional brain networks (Calhoun et al., 2014), are not captured by this approximation. Given that (1) functional brain organization comprises dynamic coordinated activity between groups of regions within and across networks and (2) neurological diseases cause widespread disruptions in connectivity across multiple networks, principled approaches that jointly incorporate statistical and temporal dependencies in a robust manner are necessary to probe the complex mechanisms and effects of brain diseases.

Recent work by Mehta et al. (2019) proposed a parametric model for characterizing trends in SPD matrices over time using temporal graphical models. In their original construction, covariance trajectories were computed on a small number of imaging-derived features over a few study visits to assess group differences in longitudinal patterns of brain changes. In addition, graph scan statistics was adapted to search over and identify distinct combinations of diffusion tensor imaging (DTI) and positron emission tomography (PET) features, along with neuropsychological scores, that stratified individuals as low- or at-risk for disease. The promising results and capabilities offered by the algorithm make it particularly well-suited to address statistical limitations inherent to many existing fMRI methods and can be optimized for use as a network-based tool to study functional brain dynamics and organization.

This dissertation aims to address the above statistical challenges for fMRI analysis and present new algorithms and techniques that leverage the geometric properties of covariance matrices in SPD space and utilize feature localization procedures that can be used as new network inference models for functional brain connectivity analyses.

In chapter 2, we demonstrate the application of combining the traditional framework for modeling functional connectivity and an extensively used network-based fMRI inference method to determine the effects of brain-computer interface (BCI) intervention on resting-state functional connectivity and motor outcomes in chronic-phase stroke patients. This

analysis motivates the need to develop more effective models for brain network analysis that rigorously account for the spatial and temporal dependencies that underpin brain function and organization.

In chapter 3, we present a novel framework that builds upon the work in Mehta et al. (2019) to rs-fMRI to identify brain networks affected in Temporal Lobe Epilepsy (TLE). Our method optimizes the algorithm for rs-fMRI analysis to characterize dFC as “trajectories” on the manifold using a Riemannian manifold regression scheme. In addition, we introduce new algorithmic capabilities that overcome challenges of computational feasibility and numerical instability that arise with a direct application of the original approach in order to effectively model high-dimensional, large-scale rs-fMRI data. This model was applied to rs-fMRI data from patients with Temporal Lobe Epilepsy (TLE) and healthy control subjects to characterize the Epilepsy connectome. Importantly, we show that our proposed framework provides several unique advantages over using existing analysis methods for fMRI. First, it demonstrates the utility of leveraging geometric properties of covariance matrices on the manifold to capture the spatiotemporal patterns in dFC as covariance trajectories. Second, it offers a principled approach to go beyond connection-level group differences and search over and localize discriminative subsets of temporally covarying features associated with disease in an efficient, statistically rigorous and interpretable manner. To the best of our knowledge, this is the first application of scan statistics to fMRI analysis, which our results demonstrate is a valuable tool for network analysis of functional connectivity dynamics.

In chapter 4, we extend the method developed in chapter 3 to detect differential effects in functional connectivity patterns between patients with Alzheimer’s Disease and healthy control individuals. This work validates the utility of the framework to identify relevant and discriminative subsets of features between clinical populations where the statistical signal may be weak due to a small sample size with a large number of features to account for.

Chapter 2

Determining the effects of BCI therapy with FES on chronic stroke patients using traditional statistical methods for functional connectivity analysis

A.M. Sinha, V.A. Nair, V. Prabhakaran. BCI Training with FES: Facilitating Changes in Interhemispheric Functional Connectivity and Motor Outcomes Post-Stroke. *Front. Hum. Neurosci.* 15.

2.1 Introduction

Approximately 800,000 people experience a new or recurrent stroke in the United States each year (Benjamin et al., 2017). An estimated 80% of survivors live with upper extremity hemiparesis that significantly impacts their independence in performing daily activities and overall quality of life (Brauer et al., 2013), constituting stroke as a leading cause of acquired long-term disability. During the recovery phase of stroke, the primary standards of care include physiotherapy and/or occupational therapy. Unfortunately, these treatment regimens only provide patients with partial motor recovery, resulting in learned non-use of the affected limb and eventual further loss of motor function (Ballester et al., 2016). To address and solve this unmet need for more effective therapies, there is a concerted effort to develop alternative approaches to restore upper limb motor function post-stroke. Several innovative therapeutic strategies, such as transcranial direct current stimulation (Kang et al., 2016), mirror therapy (Michielsen et al., 2011), robot-assisted training (Trujillo et al., 2017; Vahdat et al., 2019) and constraint-induced movement therapy (Lang et al., 2013) have emerged as promising techniques for stroke rehabilitation. Despite encouraging results shown by these and other studies, there is large variability in reported changes of neuroplasticity and recovery outcomes associated with these approaches. Therefore, it is crucial that we more deeply further investigate the efficacy of these and other methods to determine which rehabilitation approaches can offer maximal benefit for individuals recovering from stroke.

Recent advances in electroencephalography (EEG)-based brain-computer interface (BCI) offer new and potentially effective rehabilitative approaches to induce neural plasticity and restore motor function. These types of non-invasive BCI systems detect and translate a user's electrophysiological signals into meaningful outputs in real-time to control external devices, such as computers or prosthetics. Importantly, these adaptive and personalized neurofeedback systems provide an alternative means of communication for patients with motor disabilities, as individuals can engage with the BCI system in a manner that is not contingent

on peripheral motor control, effectively circumventing their impaired neuromuscular system. To date, many studies have observed clinical improvements in both upper limb motor function (Ang et al., 2015; Bajaj et al., 2015; Bundy et al., 2017; Ramos-Murguialday et al., 2019; Soekadar et al., 2015) and enhanced neural plasticity (Broetz et al., 2010; Mukaino et al., 2014; Ono et al., 2014) associated with BCI training. A number of BCI systems have been coupled with functional electrical stimulation (FES), a standard modality in stroke rehabilitation protocols. Electrical current is applied over paralyzed muscles to activate nerves and stimulate muscle contraction, with the goal to improve hand function and dexterity. Previous studies have shown that these integrated BCI-FES systems can foster recovery of both upper and lower limb function in the stroke survivor population (Biasucci et al., 2018; Cho et al., 2018; Daly et al., 2009; Do et al., 2012; Tsuchimoto et al., 2019).

Resting-state functional magnetic resonance imaging (rs-fMRI) has gained widespread use as a powerful neuroimaging modality to probe and characterize brain connectivity with high spatial resolution. Resting-state functional connectivity (rsFC) measures temporal correlations between fluctuations in the spontaneous, low-frequency blood oxygenation level-dependent (BOLD) signal across distributed brain regions in a task-free setting. With rsFC, we can circumvent challenges with acquiring task fMRI data from patients with neurological diseases and study coactivating patterns that are consistent with and resemble functional networks active during tasks (Biswal et al., 1995). A large and growing number of studies have demonstrated the promise and utility of rsFC to capture and monitor neural reorganization (Baker et al., 2014; Urbin et al., 2014), and yielded important clinical insights into the underlying pathophysiological mechanisms and effects of disease, as well as response to treatment (Du et al., 2018). With its demonstrated use to study intrinsic brain connectivity dynamics, rsFC can serve as a means to monitor and evaluate the effects of stroke rehabilitation strategies on functional motor recovery.

Recently, we have shown that task-based functional connectivity and diffusion tensor imaging are useful in studying neural reorganization in patients with stroke who received

BCI neurorehabilitation (Song et al., 2015; Young et al., 2014b). Several other works have reported beneficial effects in electrophysiological changes and functional motor recovery (Bisiucci et al., 2018; Bundy et al., 2017; Pichiorri et al., 2015; Remsik et al., 2019) associated with the use of BCI-controlled systems. Notably, in both spontaneous recovery and training-mediated stroke rehabilitation, studies have observed increased activation in the contralateral and ipsilesional hemispheres separately and restoration of interhemispheric balance (Dodd et al., 2017)). However, these underlying neuroplastic changes in interhemispheric and intrahemispheric rsFC in patients with stroke who undergo BCI intervention with FES are not fully understood. Even further, our understanding of how changes in rsFC relate to behavioral outcomes of motor ability with this form of BCI intervention is limited. Given that coordinated interactions among groups of regions underpin brain function and the underlying mechanisms of recovery processes, it is important to go beyond individual connections and investigate how rsFC network patterns relate to observed behavioral changes. In the stroke survivor population, there is considerable heterogeneity in stroke severity and degree of motor impairment, which invariably affect recovery potential. Therefore, it is critical that we have a detailed understanding of brain-behavior relationships associated with this intervention to both evaluate its therapeutic utility and further optimize neuromodulatory training to facilitate maximal motor recovery for patients after stroke.

2.1.1 Overview of study

This aim of this study was to assess changes in rsFC and motor outcomes in patients of stroke with upper extremity motor deficits who completed EEG-based BCI intervention paired with FES. In the BCI paradigm, participants modulated sensorimotor rhythms, Mu (8 – 12 Hz) and Beta (18 – 25 Hz), using attempted hand movement to play a computer game while receiving multimodal feedback. Here, we performed group-level analysis of (1) changes in rsFC between brain regions involved in planning, initiating and executing motor commands and (2) changes in behavioral outcome measures related to motor function after BCI inter-

vention. Results were subsequently used to identify correlations between observable changes in rsFC and behavioral improvements. Given previous findings of increased interhemispheric connectivity in spontaneous recovery and after treatment that correlated with motor recovery (Fan et al., 2015; Urbin et al., 2014; Varkuti et al., 2013), it was hypothesized that there would be significant increases in interhemispheric rsFC and behavioral performance from baseline to post-intervention following training with the BCI system. In a similar vein, we hypothesized that these changes in rsFC between time points would correlate with gains in behavioral outcomes and have observable effects that persist one month after intervention.

2.2 Materials and methods

2.2.1 Participants

Participants were recruited as part of an ongoing stroke rehabilitation study that is investigating the effects of EEG-based BCI with FES intervention on upper extremity motor recovery. The study was approved by Health Sciences Institutional Review Board of the University of Wisconsin-Madison and is registered with ClinicalTrials.gov with the assigned identifier, NCT02098265. Eligibility criteria were: (1) at least 18 years or older; (2) persistent upper extremity motor impairment resulting from ischemic or hemorrhagic stroke; (3) ability to provide written informed consent. Exclusion criteria were: (1) concomitant neurodegenerative or other neurological disorders; (2) psychiatric disorders or cognitive deficits that would preclude a subject's ability to provide informed consent; (3) pregnant or likely to become pregnant during the study; (4) allergies to electrode gel, metal and/or surgical tape; (5) contraindications to MRI; (6) concurrent treatment for infectious disease. There was no cut-off requirement related to upper extremity motor impairment to participate in the BCI intervention. All subjects provided written informed consent prior to enrollment in the study.

In this study, the subject cohort was limited to patients who were in the chronic stage

Table 2.1: Demographic information of subjects.

Subject	Age Range (years)	Gender	Lesion side	Lesion Location	Time since stroke (months)
1	50-54	M	L	MCA	15
2	59-63	F	L	Frontal Lobe	6
3	64-68	M	L	MCA	24
4	71-75	F	L	MCA	16
6	57-61	M	L	MCA	28
7	43-47	F	R	MCA	99
8	69-73	F	R	MCA	26
9	78-82	M	R	Occipital lobe	21
10	41-45	M	L	MCA	168
11	62-66	F	R	Frontal lobe	13
12	69-73	M	R	MCA	26
13	73-77	F	R	Putamen	23
14	46-50	M	R	Pons	4
15	54-60	M	L	MCA	12
16	48-52	M	R	MCA	16
17	75-79	M	L	PVWM	22
18	67-71	M	R	Putamen	90
19	81-85	F	L	Cerebellar vermis	19
20	72-76	F	R	Prefrontal	6
21	40-44	F	R	Frontal parietal	87
22	55-59	F	R	Frontal lobe	19
23	45-49	M	R	ATL	15

Abbreviations: F, female; M, male; L, left; R, right; MCA, middle cerebral artery; PVWM, periventricular white matter; ATL, anterior temporal lobe; ARAT, Action Research Arm Test

(>4 months since stroke onset), completed at least 9 of the 15 BCI intervention sessions, completed all 4 MRI scans and neuropsychological assessments and had neuroimaging data obtained from 3T MRI scanners. Furthermore, subjects were excluded here if they presented with bilateral lesions, as additional variables could be introduced that confound the analysis. In total, 23 participants (age = 62 ± 12.8 years, 10 females) who completed BCI intervention were included in the current analysis. The average time since stroke, defined as the duration between date of stroke onset and the preliminary visit, for subjects in the cohort was 33 ± 40.5 months. Severity of upper extremity motor impairment was evaluated based on performance

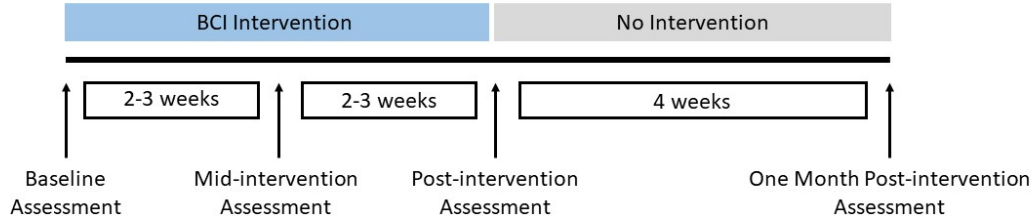


Figure 2.1: Study schedule for BCI intervention.

on the Action Research Arm Test (ARAT) (Carroll et al., 1965) at the preliminary visit and classified as follows: mild = 40 – 57 ($n = 7$), moderate = 20 – 40 ($n = 2$), severe = 0 – 20 ($n = 14$). Post-stroke handedness was assessed using the Edinburgh Handedness Inventory (Oldfield, 1971). 19 subjects were right-handed, 2 were left-handed and 2 were ambidextrous. Demographic and clinical information about the participants are summarized in Table 2.1.

2.2.2 Study design

This ongoing study has employed a permuted block randomization scheme of which details have been described previously (Mohanty et al., 2018). In the present work, we only report results based on analysis of neuroimaging and behavioral data from all subjects during from the intervention phase, which includes three distinct time points, pre-intervention, post-intervention and one month post-intervention. The study schedule for the BCI intervention is shown in Figure 2.1. This is line with the main focus of the current study, which was based on a within-subjects design, where each subject serves as his/her own control based on baseline scores, to monitor changes in functional connectivity and behavioral outcomes over time associated with BCI intervention.

2.2.3 BCI intervention

All subjects received up to 15 two-hour EEG-based BCI sessions with visual feedback and functional electrical stimulation (FES) that occurred two to three times per week. The BCI

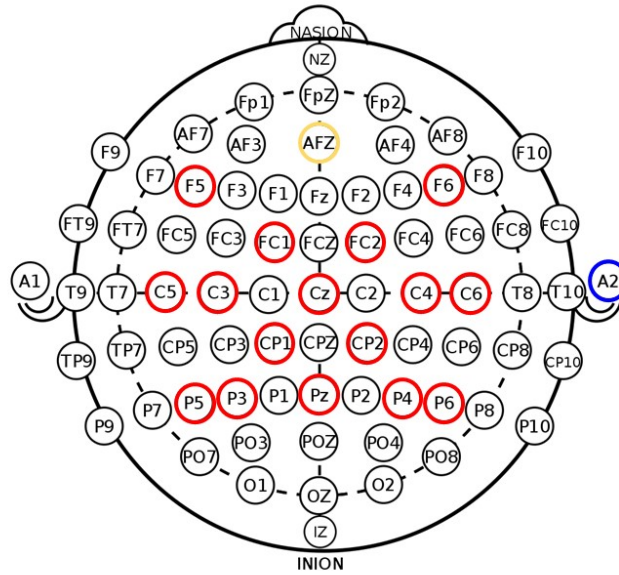


Figure 2.2: Electrode placement in 16-channel EEG cap used in BCI system (red – active electrodes, yellow – ground electrode, blue – reference site on right ear lobe) adapted from (Remsik et al., 2019). Signals from electrode channels C3 and C4 served as input into the BCI classifier to control lateral cursor movement.

system and intervention procedure are consistent with those detailed in previous studies (Wilson et al., 2009; Young et al., 2014a). Briefly, BCI interventions were administered on a computer using BCI2000 software (Schalk et al., 2004) version 2. Modifications were made to the system to incorporate tongue stimulation (Tongue Display Unit 0.130 Wicab Inc.) and FES using an LG-7500 Digital Muscle Stimulator (LGMedSupply, Cherry Hill, NJ, USA; Arduino 1.0.4). However, due to equipment-related issues, very few subjects in the overall larger study received tongue stimulation and hence the analysis and results reported here only pertain to BCI intervention with FES. EEG data were acquired using a g.GAMMA cap and amplifier (Guger Technologies), with 16 active electrodes (F5, FC1, C5, C3, CP1, P5, P3, Cz, Pz, F6, FC2, C4, C6, CP2, P4 and P6) and a reference site at the right ear lobe as shown in Figure 2.2. The system was configured according to the standard 10-20 system of electrode placement. Within BCI2000, raw EEG signals were preprocessed using a band-pass filter (0.1 – 100 Hz) and a notch filter to remove noise. The power spectrum was estimated by fitting an autoregressive model, and extracted features in Mu (8 – 12 Hz)

and Beta (18 – 25 Hz) from electrodes C3 and C4 during cued voluntary movement of the left and right hand were used as input into a linear classifier to determine lateral cursor movement.

BCI intervention sessions consisted of three parts: (1) an open-loop calibration task without any feedback, (2) a closed-loop task with visual feedback and (3) a closed-loop task with visual feedback, tongue stimulation and FES. During the open-loop calibration task, subjects were prompted with visual and auditory cues to execute right/left hand movement, imagine right/left hand movement or rest. Given that motor deficits related to grasping and releasing objects are common in patients of stroke, subjects chose between either multi-finger extension or flexion hand movement for the intervention. Calibration was performed at the beginning of each session to account for slight variability in Mu and Beta rhythms across individuals. During the calibration task, EEG activity were recorded from subjects as they performed attempted left and right hand movement to identify activation patterns in the sensorimotor cortex corresponding to voluntary movement of each hand. These patterns were saved as the EEG-based control signals for the following closed-loop task. Subjects were instructed to perform attempted movement during both the calibration and closed-loop tasks to simulate real-world tasks that they would engage in on a daily basis.

Following the calibration task, subjects performed the closed-loop task, which consisted of a cursor task game. The goal was to move a cursor (ball) toward a rectangular target that was randomly positioned on either the left or right side of the computer screen in each trial. Subjects were instructed to perform either multi-finger extension or flexion of their right or left hand to elicit real-time EEG control signals identified during calibration to control lateral cursor movement (left or right) towards the target. Here, cursor movement served as continuous visual feedback to the subject. The closed-loop task with visual feedback consisted of a minimum of 10 successful runs (8 – 12 trials per run), which subjects had to complete with at least 70% accuracy. . If performance accuracy was less than 70% after these runs, individuals completed additional trials until they consistently reached or exceeded the

necessary level of proficiency before transitioning to the next task. In the present analysis, all subjects achieved the required 70% accuracy within the first 10 runs of the closed-loop task.

Following the runs with visual feedback alone, sensorimotor rhythm-triggered FES was introduced into the closed-loop cursor task. The coupling of FES with BCI creates a direct communication pathway between the brain and peripheral stimulation device, effectively “closing the loop” between the brain and impaired muscles. Subjects also received intermittent tongue stimulation throughout the trials as reported previously (Kaczmarek, 2011; Wilson et al., 2012). FES was delivered through two 2” × 2” square electrodes that were placed on either the flexor digitorum superficialis of the subject’s forearm stimulate multi-finger flexion or the extensor digitorum communis to stimulate finger extension. The FES pulse frequency was set to 60 Hz to generate tetanic contraction with a pulse width = 150 μ s and could be adjusted in increments of 0.5 mA based on the subject’s comfort level. During trials in which the target appeared on the side of the affected arm, if EEG signals corresponding to multi-finger extension or flexion of the affected arm were detected, FES was administered to the subject. Thus, in this construction, the BCI system links the modulation of brain activity to concurrent sensory feedback. Game settings, such as target size and cursor speed, could be adjusted to vary task difficulty in order to keep subjects engaged and motivated throughout the session.

2.2.4 Data acquisition: neuroimaging

MRI scans were acquired on GE 750 3T MRI scanners (GE Healthcare, Waukesha, WI) with an 8-channel head coil. 5-minute T1-weighted anatomical scans were obtained using a BRAVO FSPGR sequence: TR = 8.16 ms, TE = 3.18 ms, TI = 450 ms, FOV = 256 mm, matrix size = 256 × 256, flip angle = 12°, number of slices = 156 and slice thickness = 1 mm. For rs-fMRI scans, subjects were instructed to remain relax and awake with their eyes closed. 10-minute rs-fMRI data were acquired using a T2*-weighted gradient – echo planar

imaging (EPI) pulse sequence: 231 volumes, TR = 2600 ms, TE = 22 ms, FOV = 224 mm, matrix size = 64×64 , flip angle = 60° , 40 axial slices and $3 \times 3 \times 3$ mm³ voxels.

2.2.5 Data acquisition: behavioral outcome measures

To assess the behavioral effects of BCI intervention, a neuropsychological battery of objective and subjective measures was administered to each participant at each time point. The primary outcome measures were the ARAT (Carroll, 1965; Lang et al., 2006) and 9-Hole Peg Test (9-HPT) (Chen et al., 2009). Scores on the ARAT, a widely used 19-measure metric quantifying upper extremity motor function in stroke recovery, were reported as total points scored out of 57 when the participant performed the task with his/her affected arm. In ARAT, the minimal detectable change (MDC) and minimally clinically important difference (MCID) were 3 points and 5.7 points, respectively (Van der Lee et al., 1999). 9-HPT is a quantitative assessment that measures finger dexterity, and scores were calculated as the average of two timed trials using the affected arm. Secondary outcome measures included the Stroke Impact Scale (SIS) (Carod-Artal et al., 2008; Duncan et al., 1999) standard domains, Strength, Activities of Daily Living (ADL), Mobility and Hand Function, and Barthel Index (Mahoney and Barthel, 1965). Following standard SIS scoring practices, SIS domain scores were scaled to adjust for the lowest possible individual raw score and raw score range.

2.2.6 Data preprocessing

Neuroimaging data were preprocessed using AFNI (Cox, 1996) and FSL (FMRIB Software Library) (www.fmrib.ox.ac.uk/fsl). Preprocessing steps included removal of the first three volumes of each scan, image despiking, slice time correction, alignment with anatomical scan, spatial smoothing at 4 mm with a full width at half maximum Gaussian kernel, transformation into MNI space (3.5 mm isotropic), motion censoring (per TR motion > 1 mm or 1°), nuisance regression (regressing out the signal from white matter) and bandpass filtering

(0.009 – 0.08 Hz). Given the ongoing controversy of global signal regression, it was not included as a preprocessing step in this work. To account for heterogeneity in lesion location among subjects, MRI scans of a left hemisphere stroke and motor impairment on the contralateral side were mirrored along the midline to generate scans of a right hemisphere stroke lesion. Thus, as a cohort, the stroke lesion was modeled in the right hemisphere, and the motor impairment was in the left upper extremity. This additional preprocessing step of mirroring MRI scans was based on the inherent assumption of symmetry in motor network activity and organization and as such are comparable as performed in previous studies (Stagg et al., 2012; Ward et al., 2003; Young et al., 2014b).

2.2.7 Functional connectivity analysis

Motor network regions of interest (ROIs) analyzed in this work are cortical and subcortical regions that are activated during visually-paced hand movements and are based on previous studies that investigated rsFC changes in participants with stroke (Grefkes et al., 2008; Nair et al., 2015). The eight ROIs were: left primary motor cortex (L. M1) (MNI coordinates: -39, -22, 57), right primary motor cortex (R. M1) ((MNI coordinates: 40, -23, 55), left premotor cortex (L. PMC) (MNI coordinates: -48, 1, 36), right premotor cortex (R. PMC) (MNI coordinates: 58, 1, 35), left supplementary motor area (L. SMA) (MNI coordinates: -6, -14, 53), right supplementary motor area (R. SMA) (MNI coordinates: 8, -14, 52), left thalamus (L. Thal) (MNI coordinates: -8, -26, 12) and right thalamus (R. Thal) (MNI coordinates: 8, -26, 12). Henceforth, ROIs located in the right hemisphere are denoted with the prefix “i” for the ipsilesional hemisphere, and ROIs located in the left hemisphere are denoted with the prefix “c” for the contralesional hemisphere. MNI coordinates for each ROI were used to create 8-mm radius spherical seeds and generate a mask for each motor network region. For each subject, fMRI BOLD timeseries data was extracted from the regions, and Pearson correlation was computed between all pairs of ROIs to compute correlation connectivity matrices. In total, there were $(8 \times (8-1))/2 = 28$ pairwise connections. Here, each (i, j) element

of the correlation matrix represented the strength of association or connectivity between the i th and j th ROI. Fisher’s r -to- z transform was applied to the correlation matrices to stabilize variance in the data, generating subject-specific z-score matrices, which were used for group-level analysis using the Network-Based Statistic (NBS) (Zalesky et al., 2010) toolbox.

2.2.8 Group-level analysis

With the aim to investigate the effects of BCI intervention on motor network functional connectivity at the group-level, we combined NBS with generalized estimating equations (GEE) (Hanley et al., 2003) to identify statistically significant connections at each time point and assess how they changed over time. We briefly describe the procedure for performing group comparisons of functional connectivity using NBS, a non-parametric approach that identifies subnetworks of functionally connected ROIs. First, mass univariate t-tests are performed on each pairwise connection to compute a corresponding t-statistic. NBS then generates a sparse graph containing only connections that exceed a predefined t-statistic threshold, termed suprathreshold connections, and uses a breadth-first search to identify connected components within the subset identified. Permutation testing is performed on the components to identify subnetworks that are statistically significant such that we can reject the null hypothesis of a zero mean, and a family-wise error-corrected p-value is calculated for each subnetwork of connections deemed significant. Full details of this method can be found in Hanley et al. (2003). Here, we used NBS with one-sample t -tests (t -statistic threshold = 2.0, $p < 0.05$, permutations = 5,000) run on the z-score matrices to identify statistically significant connections at the group-level for each of the three time points. For each subject, the mean z-score was calculated by averaging the strengths of the significant connections identified at each time point. Similar to previous work that investigated global changes in intrahemispheric and interhemispheric functional connectivity after stroke (Lee et al., 2018; Nair et al., 2015), connections were organized into intrahemispheric connectivity (connections within the same hemisphere), interhemispheric connectivity (connections

between both hemispheres) and network connectivity (combined intrahemispheric and inter-hemispheric connections) for each subject and time point for subsequent analysis.

Additional group-level analyses of rsFC and behavioral outcome measures were performed using GEE with a significance threshold of $p < 0.05$. GEE, an extension of the generalized linear model, is a semi-parametric approach for longitudinal analysis of correlated continuous or categorical response variables, in which there are no underlying assumptions related to the distribution of the data (i.e. normal, binomial, etc.). Unlike the mixed effects model, which uses random effects to quantify correlation between repeated measures at the individual-level, GEE uses changes in the mean group responses to generate population averaged models. “Time since stroke” (months) and baseline scores for each assessment were included as covariates. Changes in motor network rsFC were further analyzed to identify correlations with changes in behavioral outcomes from pre-intervention to both post- and one-month post-intervention. Subjects that had a change in rsFC \geq two standard deviations away from the mean and/or exhibited ceiling or floor effects were deemed outliers and excluded in the group-level analyses.

2.3 Results

2.3.1 Functional connectivity in the motor network

At baseline, one-sample t-tests revealed that the top three significant connections identified by NBS at the group level were: i.M1 – i.SMA (t -statistic = 8.12), i.M1 – c.SMA (t -statistic = 8.14) and c.SMA – i.SMA (t -statistic = 10.48). At post-intervention, the three strongest connections included: i.M1 – c.SMA (t -statistic = 9.06), i.M1 – i.SMA (t -statistic = 9.17) and c.SMA – i.SMA (t -statistic = 10.30). At one-month post-intervention, the top three significant connections identified were: i.M1 – c.SMA (t -statistic = 7.98), i.M1 – i.SMA (t -statistic = 8.45) and c.SMA – i.SMA (t -statistic = 10.77). NBS identified 15 significant connections at each time point, which are grouped at the interhemispheric and intrahemi-

Table 2.2: Significant interhemispheric and intrahemispheric connections at each time point identified using NBS (Zalesky et al. 2010) based on t-statistic ($p < 0.05$).

	Pre-	Post-	One Month Post-
<i>Interhemispheric connections</i>			
c.PMC - i.SMA	2.98	4.35	3.96
c.M1 - i.PMC	3.24	4.65	4.27
i.M1 - c.PMC	3.55	4.66	3.07
c.PMC - i.PMC	4.02	5.07	4.03
c.M1 - i.SMA	4.99	5.57	5.65
i.PMC - c.SMA	5.20	6.50	5.77
c.M1 - i.M1	5.30	6.15	6.06
i.M1 - c.SMA	8.14	9.06	7.98
c.SMA - i.SMA	10.48	10.30	10.77
<i>Intrahemispheric connections</i>			
c.M1 - c.PMC	3.08	3.75	4.47
c.PMC - c.SMA	3.38	4.26	4.14
i.PMC - i.SMA	5.57	6.47	5.69
c.M1 - c.SMA	6.89	7.16	7.17
i.M1 - i.PMC	7.14	7.53	7.32
i.M1 - i.SMA	8.12	9.17	8.45

Abbreviations: i., ipsilesional; c., contralesional

spheric level in Table 2.2. To examine changes in rsFC in the motor network changed after intervention, we investigated how the significance of connections changed from baseline to post- and one-month post-intervention.

As some connections increased in strength while others decreased throughout and after intervention, it is not surprising that paired t-tests of connections using permutation testing from baseline to each time point did not reveal significance. However, GEE analysis revealed significant group-level increases in rsFC from baseline to immediately post-intervention for average network connectivity ($p = 0.000000392$), intrahemispheric connectivity ($p = 0.01$) and interhemispheric connectivity ($p = 0.026$). Furthermore, there was a markedly significant increase in average network connectivity strength that persisted from pre- to one month-

Table 2.3: GEE analysis of behavioral outcome measures.* $0.05 < p < 0.1$.

Outcome measure	Time	N	Improvement Mean (SD)	GEE p -value
Barthel Index	Pre- to post-	23	2.3(2.2)	0.057*
	Pre- to one month post-	23	5.7(7.8)	0.180
SIS Strength	Pre- to post-	23	4.9(14.2)	0.097*
	Pre- to one month post-	23	7.1(13.7)	0.013
SIS ADL	Pre- to post-	23	4.6(10.9)	0.044
	Pre- to one month post-	23	4.3(11.2)	0.062*
SIS Mobility	Pre- to post-	23	5.2(12.2)	0.041
	Pre- to one month post-	23	6.1(12.5)	0.019
SIS Hand Function	Pre- to post-	23	2.0(11.5)	0.414
	Pre- to one month post-	23	2.5(11.6)	0.303
ARAT (affected)	Pre- to post-	19	1.6(5.2)	0.187
	Pre- to one month post-	19	3.0(5.6)	0.012
9-HPT (affected)	Pre- to post-	7	-0.16(16.1)	0.413
	Pre- to one month post-	7	-2.6(8.7)	0.431

post-intervention ($p = 0.000358$), but not for intrahemispheric connectivity ($p = 0.053$) or interhemispheric connectivity ($p = 0.198$).

2.3.2 Behavioral outcome analysis

Group-level analysis of behavioral measures using GEE revealed significant improvements on SIS ADL ($p = 0.044$) and SIS Mobility ($p = 0.041$) from baseline to post-intervention. Furthermore, there was a trend towards significance for improvement in Barthel Index ($p = 0.057$) from baseline to post-intervention. While 3 subjects improved by MDC (3 points) or MCID (5.7 points) on ARAT from pre-intervention to post-intervention, there was not a significant increase on ARAT as a group. However, from baseline to one month post-intervention, participants significantly improved on ARAT using the affected arm ($p = 0.023$),

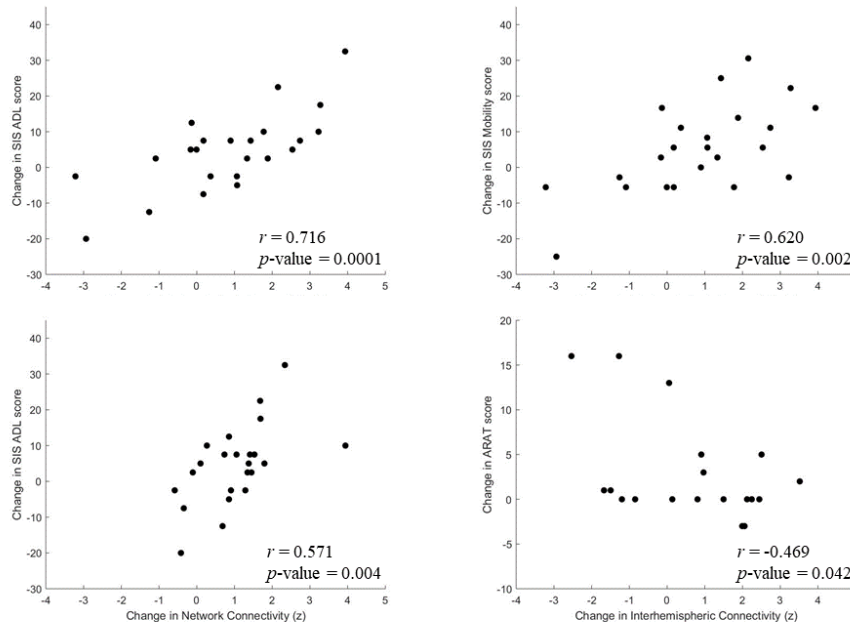


Figure 2.3: From pre-intervention to post-intervention, significant correlations were identified between changes in (A) SIS ADL and interhemispheric connectivity, (B) SIS Mobility and interhemispheric connectivity and (C) SIS ADL and average network connectivity. (D) From pre-intervention to one month post-intervention, changes in ARAT negatively correlated with interhemispheric connectivity changes.

with 6 subjects improving by MDC or MCID. In addition, patients exhibited significant increases in SIS Strength ($p = 0.013$) and SIS Mobility ($p = 0.019$) and a trend towards significance on SIS ADL ($p = 0.062$) between time points. It should be noted that group performance on ARAT was only analyzed from subjects that could perform the assessment with the affected arm ($n=19$). Full results of group-level changes and improvement scores in primary and secondary outcome measures from pre-intervention to post- and one month post-intervention are presented in Table 2.3.

2.3.3 Associations between changes in functional connectivity and behavioral outcome measures

Previous studies primarily focused on changes in interhemispheric functional connectivity following stroke rehabilitation (Fan et al., 2015; Varkuti et al., 2013; Young et al., 2014b),

Table 2.4: Correlations between change in average and interhemispheric rsFC and behavior. * $0.05 < p < 0.1$.

	N	Pearson's r	p -value
<i>Average network connectivity</i>			
<i>Pre-intervention to post-intervention</i>			
SIS Strength	23	0.329	0.125
SIS ADL	23	0.571	0.004
SIS Mobility	23	0.243	0.263
SIS Hand Function	23	-0.021	0.924
ARAT (affected)	19	0.226	0.352
9-HPT (affected)	7	-0.508	0.224
<i>Average network connectivity</i>			
<i>Pre-intervention to one month post-intervention</i>			
SIS Strength	23	0.150	0.494
SIS ADL	23	-0.268	0.217
SIS Mobility	23	0.176	0.442
SIS Hand Function	23	-0.352	0.100
ARAT (affected)	19	-0.273	0.258
9-HPT (affected)	7	-0.259	0.575
<i>Interhemispheric connectivity</i>			
<i>Pre-intervention to post-intervention</i>			
SIS Strength	23	0.206	
SIS ADL	23	0.716	0.0001
SIS Mobility	23	0.620	0.002
SIS Hand Function	23	0.301	0.163
ARAT (affected)	19	0.034	0.891
9-HPT (affected)	7	-0.695	0.083*
<i>Interhemispheric connectivity</i>			
<i>Pre-intervention to one month post-intervention</i>			
SIS Strength	23	0.072	0.743
SIS ADL	23	0.01	0.965
SIS Mobility	23	0.084	0.703
SIS Hand Function	23	-0.257	0.237
ARAT (affected)	19	-0.469	0.042
9-HPT (affected)	7	-0.398	0.377

however, we explored network, intrahemispheric and interhemispheric dynamics for subsequent group-level correlation analysis with behavioral performance. From baseline, or pre-intervention, to post-intervention, we identified positive correlations between improvements in SIS ADL and increases in average network connectivity ($r = 0.571$, $p = 0.004$) and functional gains in SIS ADL ($r = 0.716$, $p = 0.0001$) and SIS Mobility ($r = 0.620$, $p = 0.002$) with changes in interhemispheric rsFC, which are shown in Figure 2.3. Moreover, there was a trend towards significance in correlation between interhemispheric connectivity and 9-HPT for the affected arm ($r = -0.695$, $p = 0.083$) to post-intervention. No correlations were identified between intrahemispheric connectivity and outcome measures from baseline to any time point. From baseline to one month post-intervention, changes in interhemispheric connectivity negatively correlated with ARAT ($r = -0.469$, $p = 0.042$). Results of correlation analyses of rsFC and behavioral changes after BCI intervention are listed in Table 2.4.

2.4 Discussion

The objective of this study was to evaluate the effects of EEG-based BCI intervention with FES on intrinsic connectivity dynamics and upper limb motor recovery post-stroke. We showed that from baseline to post-intervention, there were significant changes in network, intrahemispheric and interhemispheric connectivity and improvements in objective and patient-reported measures that persisted to one month post-intervention. Notably, from baseline to post-intervention, changes in interhemispheric connectivity correlated with gains in SIS ADL and Mobility. Furthermore, interhemispheric connectivity changes negatively correlated with ARAT from baseline to one month after intervention.

2.4.1 Functional connectivity changes associated with intervention

We see BCI-training associated changes in rsFC at the connection level from baseline to post- and one-month post-intervention, as indicated by strengthening and weakening of connections based on increases and decreases in their t-statistics, respectively. In particular, the contralesional and ipsilesional supplementary motor areas and primary motor cortex showed significantly increased interhemispheric and intrahemispheric (within the ipsilesional hemisphere) coupling of BOLD activity, which aligns with previous evidence of improvement in upper-limb recovery following BCI intervention (Varkuti et al., 2013). In particular, the ipsilesional primary motor cortex was identified in several significant connections across time points, which is consistent with published studies that found it to be a main target for stroke neurorehabilitation (Buetefisch, 2015; Tsuchimoto et al., 2019). Moreover, the supplementary motor areas have been shown to play a functional role in both motor imagery and motor planning (Min et al., 2020), therefore, increases in rsFC strength exhibited between the ipsilesional and contralesional supplementary motor areas after BCI training may be a form of adaptive motor network reorganization. In addition, connectivity between the ipsilesional and contralesional primary motor cortex strengthened after intervention, which supports previous findings of increases in M1-M1 connectivity after rehabilitation that correlated with improved recovery outcomes (Fan et al., 2015; Min et al., 2020). Furthermore, connectivity analysis revealed asymmetry in rsFC, with more significant connections identified in the contralesional hemisphere than in the ipsilesional hemisphere. This may indicate a greater role of the contralesional hemisphere in neural plasticity related to motor recovery, given the severity and extent of stroke-induced damage in the ipsilesional hemisphere.

As hypothesized, there were notable increases in network and interhemispheric functional connectivity from baseline to post-intervention. These results are consistent with recent findings demonstrating associations between decreased interhemispheric rsFC and

motor impairment that significantly increase during post-stroke motor recovery. Therefore, BCI intervention may be beneficial in strengthening functional connections to restore sensorimotor control. Currently, there is no definitive consensus on how to optimally activate or inhibit the contralesional or ipsilesional hemisphere for stroke recovery (Dodd et al., 2017), however, these findings provide evidence to explore targeted interventions involving interhemispheric connectivity to foster neuroplasticity for regaining motor function. Nevertheless, future studies that assess rsFC interhemispheric and intrahemispheric dynamics throughout intervention will more comprehensively elucidate the roles of the contralesional and ipsilesional hemispheres in stroke recovery.

2.4.2 Improvements in behavioral outcomes associated with intervention

Our results also showed significant group-level improvements in outcome measures, including ARAT and SIS domains, that are preserved long-term after completing BCI intervention. Notably, behavioral improvements in ARAT of MDC/MCID was observed in 3 subjects from baseline to post-intervention and 6 subjects from baseline to one month post-intervention. This suggests that BCI-mediated intervention may have therapeutic benefits for individuals with varying degrees of motor deficits that are quantifiable by standardized objective measures. It is acknowledged that some individuals were unable to perform the primary outcome measures due to severity of motor impairment or were excluded due to floor/ceiling effects, which affected statistical power in group-level analyses. Furthermore, the observed improvement in SIS domains is promising, as this may indicate that subjects believe that they are regaining autonomy in daily activities and have improved quality of life after participating in BCI interventions. These results should be further validated using additional objective metrics, such as the Fugl-Meyer Assessment, that can more holistically evaluate motor impairment and recovery after intervention.

2.4.3 Relationship between changes in functional connectivity and functional outcomes

We then aimed to identify brain-behavior correlations based on functional interactions in the motor network responsible for planning and execution of hand movement at the network and interhemispheric level. Notably, increases in interhemispheric connectivity positively correlated with gains in SIS ADL and Mobility from baseline to post-intervention, which is in line with previous work that demonstrated the predictive value of interhemispheric rsFC for upper limb motor recovery after stroke (Min et al., 2020). Furthermore, disruptions in coordinated interhemispheric connectivity have been shown to be associated with impaired upper extremity motor function after stroke (Carter et al., 2010; Dimyan and Cohen, 2011; Murase et al., 2004). Hence, the observed increases in rsFC may be indicative of neural reorganization supporting post-stroke motor recovery. In addition, changes in interhemispheric connectivity negatively correlated with improvements in ARAT from baseline to one month post-intervention. This may suggest that sustained effects of intervention are evident in behavioral improvements, however, cortical reorganization is occurring again after discontinuation of BCI intervention. Future studies should focus on disentangling this to determine if more frequent or regular participation in BCI intervention are required to induce sustained changes in both neuroplasticity and motor function. Interestingly, several severely impaired patients were unable to perform the ARAT or 9-HPT, however, they exhibited higher increases in interhemispheric and average network connectivity that correlated with larger improvements in SIS domains relative to mild and moderate patients. It is possible that the present objective measures may not be sufficient for assessing motor function across all degrees of motor deficits, albeit these findings provide evidence that patients with severe upper extremity impairments can receive some beneficial effects from BCI intervention based on the measures evaluated here. In addition, the trend towards significance in correlation between interhemispheric rsFC and 9-HPT from baseline to post-intervention may

indicate that BCI training is beneficial for improving hand dexterity. However, the current analysis was limited in statistical power due to the number of subjects able to complete the task. It is worth noting that patients included in the analysis here were ≥ 4 months post-stroke, therefore, it is unlikely that spontaneous neurobiological recovery confounded any observed changes associated with the intervention. Overall, these results suggest that linking BCI training with somatosensory feedback may be an effective restorative therapy that can promote neuroplasticity and functional upper limb motor recovery after stroke.

It is important to emphasize that patient-reported measures are valuable in evaluating the impact of stroke and treatment, as they can overcome the limitations of floor or ceiling effects commonly observed with standard scales, such as ARAT, Barthel Index and Fugl-Meyer Assessment. Moreover, these subjective measures can be sensitive to quantifying the extent and impact of stroke and rehabilitation in patients with minimal or severe impairment that may otherwise not be measurable with standard scales (Stewart and Cramer, 2013). Furthermore, patient-reported measures provide important insights into disease effects across domains of health that impact patients' daily activities and afford a more comprehensive understanding of patient perception of functional status and recovery progress (Katzan et al., 2017; Richardson et al., 2016). Overall, the correlations between increased motor network connectivity and outcome measures suggest that functional reorganization associated with BCI intervention may reflect improvements in patient ability to participate in daily motor-related tasks and enhanced quality of life. It is possible that in the current population analyzed, these effects cannot be fully captured using clinical measures that require fine motor control. Nonetheless, these findings suggest that interhemispheric interactions within the motor network correlate with behavioral improvements and should be targeted for future optimization of BCI training with FES to facilitate neurological and upper extremity motor recovery for patients after stroke.

2.4.4 Limitations

This study has a number of limitations that should be noted. The analysis was based on a relatively small sample size with a heterogeneous patient population in terms of time since stroke, stroke lesion location and degree of upper extremity impairment. In addition, several subjects had severe motor impairments that precluded them from completing the objective assessments, which reduced statistical power in group-level analyses. However, it is important to note that challenges related to patient recruitment and retention for these longitudinal studies invariably limits the sample size that can be assessed to discern therapeutic effects on stroke recovery. Even so, the size of the patient cohort analyzed here is considerably larger than similar studies in the literature. Nonetheless, these findings were robust enough to show significant changes in rsFC and behavioral outcome measures after BCI intervention, with a number of subjects exhibiting meaningful clinical improvements in functional outcomes. This may suggest that subjects with varying degrees of motor impairment can likely benefit from this form of BCI rehabilitation to regain autonomy in daily life. Future studies should focus on a larger and more homogeneous population to both replicate and validate the present results and delineate the effects of BCI intervention on different subgroups within the stroke survivor population. This could inform who can optimally benefit from BCI intervention and predict recovery potential based on chronicity and/or severity of motor deficits. Another limitation to consider is that functional connectivity was investigated in eight cortical regions involved in motor planning and execution. Other motor-related regions, such as the sensorimotor cortex, middle temporal gyrus, middle frontal gyrus, putamen and caudate, are likely involved in neuroplasticity changes underlying motor recovery and should be included in future analyses. This would provide a deeper understanding of the underlying neurophysiological mechanisms of rsFC changes that could elucidate both adaptive and maladaptive brain and behavioral changes related to BCI training. Furthermore, because the focus of this current analysis was to track changes in functional connectivity and be-

havior over time within subjects, no control group was included. However, this could be done in a future study when a sufficient number of control subjects have completed the BCI intervention protocol. In addition, it is acknowledged that factors, such as motivation to participate in research, practice effects, or repetitive use of the paretic arm in a supervised setting may have led to some of the observed changes, rather than the neurofeedback in the BCI intervention. Nonetheless, this work provides evidence that it is possible to improve motor-related outcomes in patients with chronic phase stroke, and BCI intervention may be beneficial in promoting that recovery. Taken together, the results presented here provide new evidence that it is possible to promote neuroplasticity changes and improve motor-related outcomes in patients of stroke in the chronic phase, and BCI intervention with FES may be beneficial in facilitating functional motor recovery after stroke.

2.5 Conclusions

The current study provides new evidence that suggest that non-invasive EEG-based BCI with FES intervention can facilitate changes in interhemispheric interactions and improve behavioral outcomes for patients of stroke with upper extremity impairment. The present findings are important as they indicate that patients may have functional capacity to restore motor function in the chronic stage of stroke that can be fostered through BCI intervention with somatosensory feedback, which could improve overall autonomy in daily life for survivors. Findings also build on previous results and demonstrate a relationship between changes in interhemispheric rsFC and motor improvements when evaluating BCI-mediated effects on motor recovery after stroke. Overall, the results presented here open the door to future avenues of research and customized optimization of the neuromodulatory training to facilitate cortical reorganization and improve motor recovery outcomes in patients after stroke.

Chapter 3

Characterizing the Epilepsy

Connectome via Differential

Covariance Analysis, a new

mathematical network-based inference

framework for modeling functional

connectivity

A.M. Sinha, R. Mehta, V. Nair, G. Hwang, R. Birn, V. Singh, V. Prabhakaran. Characterization of the Epilepsy Connectome via Covariance Trajectory Analysis. *Under revision.*

3.1 Introduction

Epilepsy is one of the most common neurological diseases today, affecting nearly 3.4 million people in the United States and more than 50 million people across the globe (Birbeck, 2010). Temporal lobe epilepsy (TLE) is the most prevalent form of epilepsy in adults, accounting for approximately 60% of seizures in the patient population (Télez-Zenteno and Hernández-Ronquillo, 2012). Patients with TLE experience recurrent and spontaneous seizures that originate in a localized area of the brain and propagate beyond the epileptogenic zone, resulting in widespread abnormalities in functional connectivity (Pittau et al., 2014). Therefore, a systems-level understanding of aberrant brain network dynamics is critical to fully elucidate the underlying mechanisms and effects of TLE.

Resting-state functional magnetic resonance imaging (rs-fMRI) has emerged as a valuable neuroimaging modality to investigate brain connectivity with high spatial resolution (Smith et al., 2012). Resting-state functional connectivity (rsFC) measures temporal correlations in the blood oxygenation level-dependent (BOLD) signal across spatially distributed brain regions in a task-free setting. Using rsFC, we can capture networks of coactivating regions that resemble functional networks active during tasks (Biswal et al., 1995; Smith et al., 2009) to probe the complexities of intrinsic brain activity and study functional network organization in health and disease.

Traditional rs-fMRI analysis methods assume stationarity in functional connectivity over time. However, converging evidence indicates that rsFC fluctuates on the timescale of seconds to minutes (Chang and Glover, 2010) within and across networks (Allen et al., 2014; Hutchison et al., 2013), which has shifted the focus toward dynamic functional connectivity (dFC) methods to capture these spatiotemporal patterns. The dominant method for estimating dFC is the sliding window method, in which correlation connectivity matrices are computed across consecutive, overlapping time windows. These classical methods rely on mass univariate testing to resolve statistical differences between groups at the connection-level. This

approach can pose several challenges in brain network analyses, as it does not account for statistical dependencies between features, heavily depends upon significance thresholds and may fail to identify group differences due to poor effect sizes.

Many network-based frameworks have emerged to characterize the dynamic and interconnected nature of the “chronnectome” (Calhoun et al., 2014). From a brain atlas or a data-driven-based parcellation (Leonardi et al., 2013; Liu et al., 2017), the sliding window method is often combined with clustering approaches to extract networks or “brain states” (Damaraju et al., 2014; Klugah-Brown et al., 2019; Smith et al., 2012). However, the optimal number of components or clusters is not always clear (Celebi et al., 2013; You and Park, 2021) and can yield different network or connectivity pattern representations, limiting interpretability or comparability across studies (Hutchison et al., 2013; Zhou et al., 2019). Alternative to mass univariate testing, graph theory (Chiang et al., 2016; Zhi et al., 2018) and community detection algorithms (Betzel and Bassett, 2017; Garcia et al., 2018) are often used to characterize the topology and modular structure of brain networks, albeit, summary measures can be challenging to interpret clinically, and detected subnetworks strongly rely on predefined heuristics or user-specified criteria, consequently limiting inference. Given that functional brain organization comprises spatiotemporal dependencies in connectivity, these features should be accounted for in a manner that requires minimal assumptions about the data to enable generalizability and reproducibility across studies.

A naïve approach to explore and identify discriminative sets of features that stratify groups would require iterating over all possible subsets of connections. Unfortunately, this would require a combinatorially large number of tests with a stringent multiple testing correction, and few if any feature subsets would survive the significance thresholds. What is needed is an end-to-end procedure that can efficiently “scan” over candidate groups of features and assess group differences in a statistically rigorous way. Localizing these discriminative subsets of features could reveal larger scale disruptions, key networks involved in disease and possibly be more stable and tied to behavior than individual connections (Finn

et al., 2019). However, methods that can do this in a principled and robust manner remain an open challenge.

Recent work by Mehta et al. (2019) adapted scan statistics to efficiently search over and localize feature subsets that contribute to between-group differences with theoretical guarantees. They model the trajectories of covariance matrices comprised of a small number of imaging-derived features over a few time points on the symmetric positive definite (SPD) manifold. Unfortunately, a direct application of the original method for large-scale dFC analysis is computationally infeasible, as high-dimensional covariance matrices comprising thousands of features over multiple time points need to be considered. The intensive computation of matrix inversions and decompositions necessary to both fit trajectories at that scale and utilize scan statistics become numerically unstable.

In this study, we address the aforementioned limitations by building upon and extending the above framework to rs-fMRI to identify brain networks affected in TLE. TLE is recognized as a network disorder affecting multiple brain systems, however, most work have focused on altered connectivity within the well-defined epileptogenic network. Here, we use scan statistics to localize subsets of temporally covarying connectivity features that exhibit significant group differences, where dFC is represented as covariance trajectories on the manifold. Experimental results demonstrate that, by incorporating both first and second-order statistics, our proposed framework not only detects functional differences found using conventional methods, but discovers novel brain network abnormalities associated with TLE. Notably, to the best of our knowledge, this is the first application of scan statistics to fMRI, with the other previous use in medical imaging analysis being in Mehta et al. (2019).

The main **contributions** of this work can be summarized as follows:

- We use scan statistics to localize differences in distinct subsets of first- and second-order connectivity features that map to brain networks affected in TLE.
- We build upon and extend the method in Mehta et al. (2019) to model dFC as covari-

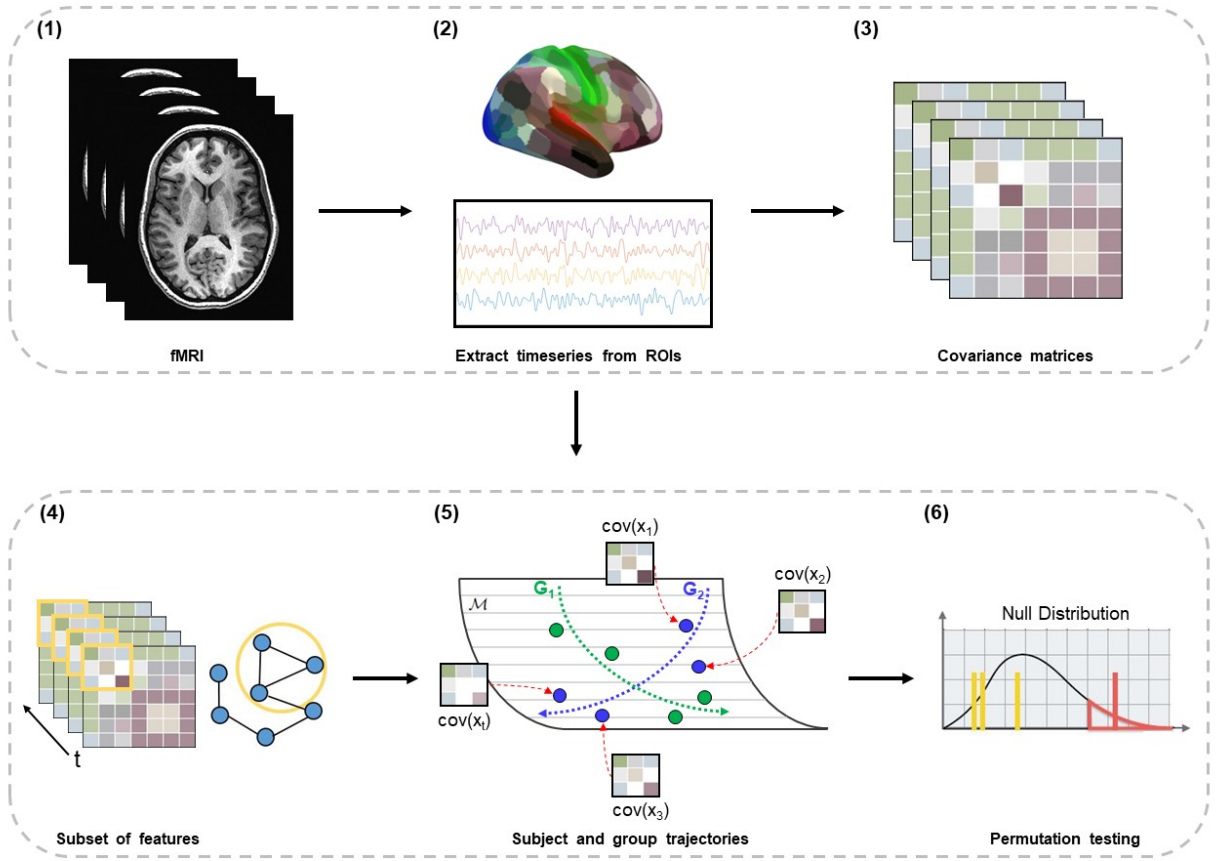


Figure 3.1: Overview of the proposed framework. The full procedure involves: (1) pre-processing fMRI data, (2) extracting timeseries from ROIs in parcellation, (3) computing subject-specific covariance matrices across time windows, (4) selecting subset of features from the input graph, (5) fitting linear and manifold regression of covariances for both groups (G_1 and G_2) and (6) computing likelihood ratio statistic and comparing against null distribution via permutation testing.

ance trajectories on Riemannian manifolds.

- We introduce a *fit-of-fits* construction to efficiently fit and compare covariance trajectories from high-dimensional rs-fMRI data.

The remainder of the paper is organized as follows. In section 3.2, we describe the proposed framework, which is illustrated in Figure 3.1. In section 3.3, we introduce the experiments and present the results. Discussion and conclusions are summarized in section 3.4.

3.2 Methods

3.2.1 Scan statistics and an alternative testing correction

Given that brain diseases cause widespread disruptions in functional interactions across networks, it is important to go beyond statistical differences in individual connections and explore *subsets of features* that differentiate patient and healthy control populations. To achieve this, we can employ scan statistics procedures developed for graphical models (Arias-Castro et al., 2011) to search over and localize subsets of connectivity features that contribute to group-level differences that would otherwise be unidentifiable with classical approaches.

We aim to answer a key question of interest in group difference hypothesis testing: are models learned on two groups the same, or are they significantly different? This problem can be formulated as a hypothesis test for each structured subset of features R of all subsets in \mathcal{R} that demonstrate a difference in any arbitrary model θ :

$$H_0 : \forall R, \theta_R^1 = \theta_R^2 \quad vs. \quad H_A : \exists R, \theta_R^1 \neq \theta_R^2 \quad (3.1)$$

In its most basic form, scan statistics involves raster scanning a window over various regions R in an image \mathcal{R} and iteratively computing a local likelihood ratio statistic L_R , analogous to the response of a filter in a neural network convolutional layer. We can extend this to the graphical setting and search over groups of connections between brain regions, which serve as our features, and compute a corresponding L_R as illustrated in Figure 3.2. The maximum of the set of individually computed local statistics, $L^* = \max_{R \in \mathcal{R}} L_R$, constitutes the scan statistic to test for group differences over \mathcal{R} . Assuming a Gaussian random field, we can construct a null hypothesis based on a threshold and identify significant between-group differences in a given subset R by comparing the local statistic L_R with the critical value. Park et al. (2015); Wang et al. (2013) demonstrated the effectiveness of this type of localization procedure for timeseries analysis.

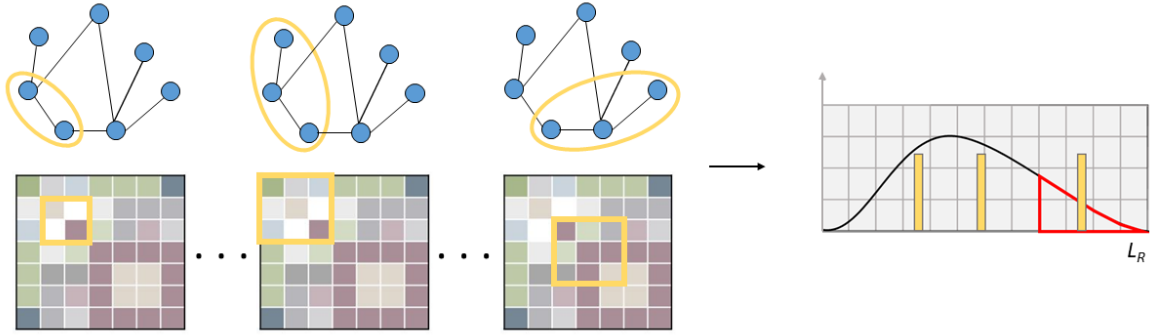


Figure 3.2: In graph scan statistics, a search procedure is iteratively performed across various subsets of features in the input graph to compute the between-group difference for each subset and obtain the local statistic.

The first step is to define each structured subset R on the graph, where R is a combination of features of which we will test the hypotheses in Equation (3.1). We should note there may not always exist a reference ground truth graph that explicitly defines subsets of features based on common properties or functionalities. When there is no prior information of how subsets of features are formed, testing each subset separately would require $2^{|\mathcal{R}|}$ number of tests and a stringent multiple testing correction. Mehta et al. (2019) addresses this by demonstrating that, with some mild assumptions of how groups of features are connected, it is in fact only necessary to search over a polynomial number of these structured subgraphs (subsets) of features. In neuroimaging analysis, however, we can use established brain atlases that partition regions into networks based on anatomical location and function to define such subsets of features.

Consider $G := (V, \mathcal{E})$ to be a graph over all subsets of features \mathcal{R} with a set of vertices V and corresponding edges \mathcal{E} . Each structured subset $R \subseteq G$ is a fully connected subgraph. We can define the input graph as an adjacency matrix, where:

$$G_{(i,j)} = \begin{cases} 1, & \text{if } i\text{th and } j\text{th ROI belong to the same network} \\ 0, & \text{otherwise} \end{cases} \quad (3.2)$$

Given that each subgraph represents a brain network with a varying number of connections, we must account for relative subgraph size when computing L_R . To achieve this, we implement a correction based on subgraph size to obtain the final likelihood ratio statistic for a given subset R as:

$$L_R^* = \frac{L_R - |E(R)|}{\sqrt{|E(R)|}} \quad (3.3)$$

Here, $|E(R)|$ denotes the number of edges within the subgraph consisting of only subset R (the number of connections within a given network).

With the size correction, L_R^* is approximately normally distributed $\mathcal{N}(0,1)$, enabling us to directly compare statistics between all subsets of features \mathcal{R} , regardless of subgraph size. In addition, the alternative correction at the group difference-level alleviates issues with multiple comparisons and ensures that we identify features that are truly significant in stratifying groups.

We then compute the alternative statistic for subset R as follows:

$$T_R^* = L_R^* - 2\sqrt{\log \frac{|E|}{|E(R)|}}, \quad (3.4)$$

where $|E|$ denotes the number of edges in the full graph (the total number of connections across all networks). This formulation allows us to compare against a single null distribution without requiring a multiple testing correction to control for the family-wise error rate, with additional guarantees on Type II error (Mehta et al., 2019). T_R^* is tested against the α -level quantile of T_R^* under the null hypothesis that there is no significant difference in the statistic computed between the two groups.

3.2.2 Likelihood Ratio Statistics

Our next step is to explicitly define a likelihood ratio statistic L_R to test the hypotheses in Equation (3.1). Henceforth, we drop the region R subscript for clarity. We can compute a general likelihood ratio statistic for our data X as:

$$L = \frac{P(X^1|\theta^1)P(X^2|\theta^2)}{P(X|\theta)} \quad (3.5)$$

Two design choices remain: defining the distribution for any $P(X|\theta)$ and the model θ itself.

The t -statistic computed in classical approaches can be seen as analogous to the likelihood ratio statistic in Equation (3.5), as it is defined over all features with a subsequent multiple testing correction and assumes both statistical independence between features and no changes in signal over time. Statistical dependencies between features is addressed using scan statistics as described above. With strategic choices for $P(X|\theta)$ and θ , we can account for dependencies over time.

For subjects $i \in \{1, \dots, N\}$ that are assumed independent, we can decompose the likelihood as a product for all subjects in a respective group (G_1, G_2):

$$L = \frac{\prod_{i \in G_1} P(X_i|\theta^1) \prod_{i \in G_2} P(X_i|\theta^2)}{\prod_{i=1}^n P(X_i|\theta)} \quad (3.6)$$

We can then choose a model for θ that is dependent over time, θ_t and calculate our sample likelihood per time point as follows:

$$P(X|\theta) = \prod_{t=1}^T \prod_{i=1}^N P(X_{i,t}|\theta_t) \quad (3.7)$$

A natural choice for θ above that provides a straightforward calculation of the likelihood ratio statistic is a Gaussian model for each time point, $\theta := (\mu, \Sigma)$. In the time-dependent

setting, $\theta_t := (\mu_t, \Sigma_t)$, and:

$$P(X|\theta) = \prod_{t=1}^T \prod_{i=1}^N P(X_{i,t}|\mu_t, \Sigma_t) \quad (3.8)$$

where our model is entirely defined by $\theta := \{\mu_t, \Sigma_t\}_{t=1}^T$.

A number of methods could be employed to estimate the Gaussian parameters in the above construction, the simplest of which is to slice the data by T and compute the empirical means and covariances. This approach, however, does not fully address the inherent dependence between time points. Instead, we could directly estimate all parameters concurrently to capture any underlying relationships of brain network interactions that may evolve over time. Next, we describe one such estimation method for fitting these parameters.

3.2.3 Estimating μ_t, Σ_t via Regression

To address the above challenges, we can define our model parameters by a best fit regression. If two separate linear models fit the data better than a single one with respect to the likelihood ratio statistic, we can conclude that the group-level “trajectories” are different.

Let $t \in \{0, 1, \dots, T\}$ be a given time point and $X_{i,t}$ be subject i 's data at time t . We can estimate our μ_t by solving the regression: $X_{i,t} = \beta_0 + \beta_1 t + \epsilon$ using standard least squares estimation with a Gaussian noise assumption on ϵ and calculate our final estimate as $\hat{\mu}_t = \hat{\beta}_0 + \hat{\beta}_1 t$.

A naïve approach to estimate Σ_t in Equation (3.8) would be to fit a regression as above for each connection in the covariance matrix over all subjects in a given group:

$$\Sigma_{j,k,t} = \beta_{0,j,k} + \beta_{1,j,k} t + \epsilon \quad (3.9)$$

Here, samples for fitting this model are pairs of $(t, \Sigma_{j,k,t})$, where (j, k) corresponds to an individual element in the covariance matrix over all subjects at time t . We can again fit a

group-specific model using a least squares estimation for each element (j, k) as follows:

$$\beta_{0,j,k}, \beta_{1,j,k} = \min_{\beta_0, \beta_1} \sum_t (\Sigma_{j,k,t} - (\beta_0 + \beta_1 t))^2 \quad (3.10)$$

While Equation (3.10) incorporates temporal dependencies between features, each connection is still statistically independent. If we need to consider a large number of features, it becomes computationally infeasible to account for all statistical interdependencies using the model above. To overcome this, we can leverage the geometric properties of covariance matrices and extend these methods directly to the ‘SPD space’ using Riemannian manifold regression.

Functional connectivity matrices can be represented as SPD matrices that form a Riemannian manifold, allowing us to perform statistical analysis on the matrices on the manifold. Next, we briefly discuss basic notions in Riemannian geometry. A Riemannian manifold is a differential manifold \mathcal{M} , equipped with a tangent space $T_{y_i}\mathcal{M}$ at a point $y_i \in \mathcal{M}$. Analogous to straight lines in Euclidean space, the locally shortest path connecting two points on a Riemannian manifold is the geodesic curve. This geodesic curve will define the temporal trajectory of the functional connectivity covariance matrices in SPD space. The exponential map, $\text{Exp}(y_i, \cdot) : T_{y_i}\mathcal{M} \rightarrow \mathcal{M}$, projects a tangent vector at base point y_i to a point on the manifold along the geodesic curve. Using these mathematical operations, we can go between the manifold space of the SPD matrices and the tangent space of covariate or predictor variables. Refer to You and Park (2021) for brief preliminaries of Riemannian geometry in fMRI analysis and Lee (2006) for a complete review of Riemannian manifolds.

Consider again the sample pairs above, but rather than treating each (i, j) element separately, now our outcome variable is the entire covariance matrix Σ . Here, our goal is to solve for the parameters of the manifold regression, so we can rewrite Equation (3.10) as:

$$\min_{b \in \mathcal{M}, \forall j, \mathcal{V} \in T_b \mathcal{M}} \frac{1}{2} \sum_t d(\text{Exp}(b, \mathcal{V}t), \Sigma_t)^2 \quad (3.11)$$

where $d(\cdot, \cdot)$ is the geodesic distance (length of shortest path) on the SPD manifold, and $Exp(\cdot, \cdot)$ is the exponential map (moving from the tangent space to the manifold). The parameters b, V are defined by the base point $b \in \mathcal{M}$ (intercept) and the tangent vector $V \in T_b\mathcal{M}$ (slope).

The objective in Equation (3.11) is often solved using gradient descent (Du et al., 2014; Fletcher, 2013) or Markov Chain Monte Carlo methods (Cornea et al., 2017), although, the computational cost of these algorithms often renders them prohibitive in practice. To circumvent this issue, we follow the Log-Euclidean approach for the longitudinal covariance general linear model (LCGLM) described in Kim et al. (2014); Mehta et al. (2019), in which the only predictor variable is time. In addition, note that trajectories are not directly comparable in Equation (3.11), as they are defined in different tangent spaces.

Over the last decade, geodesic regression problems have been extensively studied in the context of medical imaging analysis (Banerjee et al., 2015; Du et al., 2014; Fletcher, 2013). Any reasonable scheme for fitting covariances can be used as a drop-in replacement for the schemes described here. The model fitting is a black-box with respect to our likelihood ratio scan statistic. So, while we make a particular design choice due to the structure of our problem, a practitioner could employ any number of covariance regression estimators.

3.2.4 Trajectories on high-dimensional covariance matrices

As discussed above, a direct application of the method in Mehta et al. (2019) is limited by the computational cost and numerical instability associated with modeling covariance trajectories comprising a large number of features, many time points and from a large number of subjects. High-dimensional matrix inversions and eigendecompositions for fitting group-level Karcher means and regressions become infeasible to compute in reasonable time, even with modern computational resources. Convergence to good fits also becomes a challenge, leading to group models with incomparably small likelihoods.

With these issues in mind, we introduce the following modifications. First, we define time

points as windows of data, which is one to two orders of magnitude larger than the number of study visits. Conceptually similar to Dai et al. (2019), we compute trajectories across sufficiently sized time windows, where local stationarity is assumed within each window. Second, we fit a trajectory for each subject and take appropriate aggregate statistics to define a group-level trajectory from those fits, termed *fit-of-fits*. We define a model θ_i for each subject, which provides Gaussian parameter estimates of the mean $\hat{\mu}_{i,t}$ and covariance $\hat{\Sigma}_{i,t}$ for each time point. For all subjects in a given group G , the estimate of $\hat{\mu}_t$ is computed as the empirical mean of $\hat{\mu}_{i,t}$ over subjects, where $\hat{\mu}_{i,t} = \hat{\beta}_{i,0} + \hat{\beta}_{i,1}t$ with $\hat{\beta}_{i,0}, \hat{\beta}_{i,1}$ using each time point from subject i .












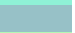




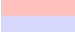

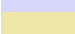



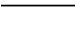
We can similarly modify the objective function in Equation (3.11) to fit a manifold regression per subject and compute an estimate of $\hat{\Sigma}_t$ as follows:

$$\hat{\Sigma}_t = \arg \min_{y \in \mathcal{M}} \sum_{i \in G} d(y, \hat{\Sigma}_{i,t})^2 \quad (3.12)$$

where $\hat{\Sigma}_{i,t}$ is the estimated fit of covariance for a specific sample $\hat{\Sigma}_{i,t} = \text{Exp}(\hat{b}_i, \hat{V}_i t)$. Solving Equation (3.12) is equivalent to computing the Karcher mean Karcher (1977) of elements on the SPD manifold. Because fitting the Karcher mean is typically iterative and can become computationally costly with a large number of subjects, we break down Equation (3.12) into fits over “hyperwindows” and compute a full Karcher mean over the hyperwindows.

Importantly, the above *fit-of-fits* construction provides significant gains in runtime efficiency for the outer hypothesis testing procedure. By estimating the null distribution of our likelihood ratio statistic using permutation testing, we simply fit a model to each subject separately and shuffle the subject fits to calculate the likelihood ratio statistic. We only recompute $\hat{\mu}_t$ and Equation (3.12) in each iteration, avoiding costly manifold regressions “in the loop”.

Table 3.1: Brain networks from Glasser et al. (2016) and FreeSurfer subcortical network

Color	Brain Network	Number of regions	Color	Brain Network	Number of regions
	Primary Visual Cortex	2		Medial Temporal Cortex	14
	Early Visual Cortex	6		Lateral Temporal Cortex	18
	Dorsal Stream	12		Temporal-Parietal-Occipital Junction	10
	Ventral Stream	14		Superior Parietal and IPS Cortex	20
	MT+ Complex and Neighbors	18		Inferior Parietal Cortex	20
	Somatosensory and Motor Cortex	10		Posterior Cingulate Cortex	28
	Insular and Frontal Opercular Cortex	26		Anterior Cingulate and Medial Prefrontal Cortex	30
	Premotor Cortex	14		Orbital and Polar Frontal Cortex	22
	Posterior Opercular Cortex	12		Inferior Frontal Cortex	16
	Early Auditory Cortex	10		Dorsolateral Prefrontal Cortex	26
	Auditory Association Cortex	16		Subcortical	19
	Sensorimotor Associated Paracentral and Mid Cingulate Cortex	16			

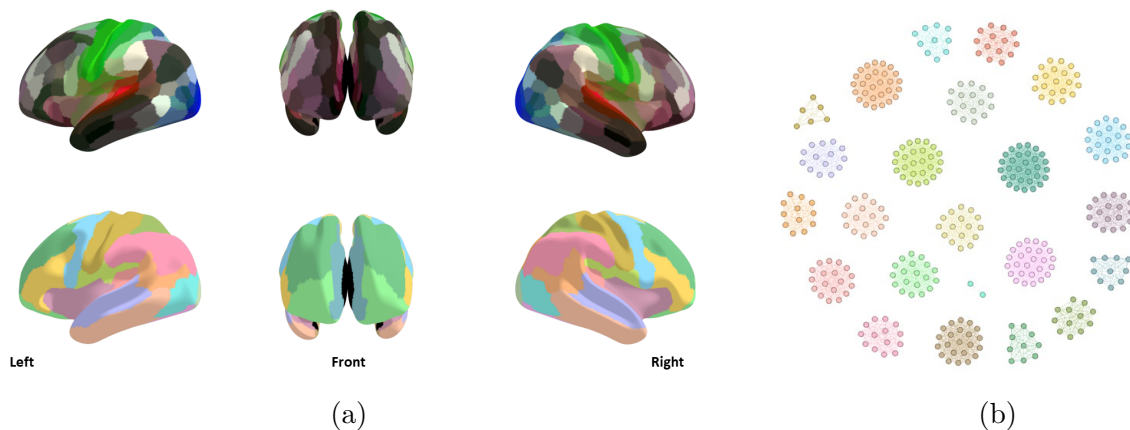


Figure 3.3: (a) 360 ROIs from the surface-based parcellation Glasser et al. (2016). (b) Graphical representation of the input graph of the parcels in their respective network.

3.3 Experiments

The following experiments are designed to investigate whether and to what extent the proposed framework can identify subsets of features that stratify patients and healthy controls. We compare our method to several existing analysis methods for fMRI as baselines.

3.3.1 Data and preprocessing

MRI scans from 87 patients with TLE and 88 healthy control subjects were obtained from two projects between the Medical College of Wisconsin and the University of Wisconsin-Madison:

Table 3.2: Demographic information of subjects.

Group	N	Gender (Male/Female)	Age (years) (Mean \pm Std)
TLE	87	36/51	39.9 \pm 12.0
Healthy Controls	88	38/50	42.3 \pm 16.1

(1) The Epilepsy Connectome Project and (2) the Alzheimer’s Disease Connectome Project. There was no significant difference between groups in terms of age, gender and education ($p > 0.26$). Demographic information is summarized in Table 3.2.

MRI data were collected on the same 3T GE 750 scanners with a Nova Medical 3T 32-channel head coil using identical imaging protocols. T1-weighted structural images were acquired using a magnetization-prepared gradient-echo sequence: repetition time (TR) = 604 ms, echo time (TE) = 2.516 ms, inversion time (TI) = 1060 ms, flip angle = 8° , field of view (FOV) = 25.6 cm, voxel size = 0.8 mm isotropic. Rs-fMRI data were acquired using whole-brain simultaneous multi-slice imaging: 8 bands, 72 slices, matrix = 104×104 , TR/TE = 802 ms/33.5 ms, flip angle = 50° , FOV = 20.8 cm and voxel size = 2 mm isotropic.

Rs-fMRI data were preprocessed using the Human Connectome Project (HCP) minimal processing pipelines version 3.4.0 (Glasser et al., 2013), which involves removal of spatial distortions, correction for subject motion, alignment to the structural data, bias field correction, normalization of the 4D image to a global mean and masking the data with the final brain mask. Additional preprocessing using AFNI (Cox, 1996) included motion regression using 12 parameters, regression-based signal removal in white matter and cerebrospinal fluid and band-pass filtering (0.01 - 0.1 Hz). In line with Cook et al. (2019); Hwang et al. (2019a), subject head motion was quantified using the derivative of root-mean-square variance over voxels (DVARs) metric (Power et al., 2012), and mean DVARs was computed across each set of scans per subject and compared between groups using a two-sample t -test ($p > 0.85$).

The BOLD timeseries were extracted from 360 cortical parcels (Glasser et al., 2016) and 19 FreeSurfer subcortical parcels for a total of $P = 379$ parcels. Parcels, or ROIs, are grouped

into one of 23 networks, which are listed in Table 3.1 and depicted graphically in Figure 3.3. Data from two 5-minute scans acquired during the same session were preprocessed separately, scaled to zero-mean unit variance and concatenated, resulting in 10-minute scan data (720 TRs) from all subjects in both groups.

3.3.2 Baseline comparison methods

We aim to compare our proposed methods against established statistical methods commonly used for group-level comparisons of functional connectivity. First, we perform conventional static functional connectivity (sFC) and dFC analyses and assess group differences using Network-based statistic (NBS) (Zalesky et al., 2010), a common method for network-based inference for fMRI. For sFC, Pearson correlation is computed between the timeseries of each pair of ROIs and converted to a subject-specific $P \times P$ z-score connectivity matrix for NBS. We estimate dFC using the sliding window approach with fixed window length = 125 TRs (~ 100 s) and stride = 5 TRs, as Zalesky and Breakspear (2015) recommends an appropriate window length of $1/f_{min}$. We compute a covariance matrix over each time window to obtain a $P \times P \times W$ matrix for each subject, where the number of windows $W = 121$. As in Chang and Glover (2010); Kucyi and Davis (2014), standard deviation is computed element-wise across matrices to generate subject dFC matrices for NBS. Briefly, NBS employs a mass univariate testing procedure and identifies components of connections that exhibit significant differences between groups or over time that controls for family-wise error. We apply NBS with a two-sample t -test for 5000 permutations and significance level of $p < 0.05$. Given that there is no guideline for the optimal t -stat threshold, we perform analyses using thresholds $t = 1.66$ and $t = 2.0$ to assess stability of NBS. It is not expected that every connection in a network is altered in disease, therefore, a network is deemed significant if $>50\%$ of unique regions in a network are identified in connections exhibiting significant group differences.

Second, we use a method introduced by You and Park (2021) that functions within the geometric constraints on the SPD manifold to test for group-level differences in connectivity.

Here, we use the subject-specific sFC covariance matrices from the control group a_1, \dots, a_m and patient group b_1, \dots, b_n in the SPD space. For each permutation $r \in \{1, \dots, R\}$, we (1) choose $\tilde{a}_1, \dots, \tilde{a}_m$ and $\tilde{b}_1, \dots, \tilde{b}_n$ without replacement, (2) compute the Frechet means for each group, μ_a and μ_b , using 3.12 and (3) calculate $D_{ab}^{(r)} = |\mu_{\tilde{a}_m} - \mu_{\tilde{b}_n}|$. We then obtain a p -value for each (i, j) connection as follows:

$$p(i, j) = \frac{\#\{z \in D_{ab}^{1:R}(i, j) \geq D_{ab}z(i, j)\} + 1}{R + 1} \quad (3.13)$$

and use the Benjamini-Hochberg procedure to correct for multiple comparisons. We refer the reader to You and Park (2021) for more details.

Third, we apply the scan statistics to covariance matrices estimated from the entire timeseries for each subject across both groups. The purpose of this baseline is to determine if scan statistics can identify discriminative sets of features based on *time-averaged connectivity* consistent with previous findings of networks perturbed in TLE. Furthermore, comparisons between this baseline and our proposed method will enable us to determine if the temporally covarying sets of features identified from the proposed framework result in the emergence of similar or different networks exhibiting significant group-level differences between patients and healthy control subjects.

3.3.3 Experimental setup

In order to fit trajectories at the subject- and group-level for group comparisons, we need to synchronize fMRI timeseries data across all subjects, while retaining individual variations in connectivity. This ensures that trajectories are fit on subject data aligned in time and space. To achieve this, we utilize the method in Akrami et al. (2019) to jointly find a set of orthogonal transforms to temporally align rs-fMRI data from multiple subjects. Here, we have timeseries data from each subject of size $T \times P$, where T is the number of TRs and P is the number of ROIs, which serve as input in above method to synchronize timeseries data at

the group-level. For subjects $i \in \{1, \dots, N\}$, we initialize the O_i 's with random orthogonal transformations and find the optimal set of transforms as follows:

$$\begin{aligned} \arg \min_{O_i, i \in \{1, \dots, N\}} N \sum_{i=1}^N \|(X_i O_i - G)\|^2 \\ = \sum_{j=1}^N \sum_{i < j}^N \|(X_i O_i - X_j O_j)\|^2 \end{aligned} \quad (3.14)$$

Each O_i minimizes the joint cost $\sum_{i=1}^N \|X_i O_i - G\|^2$, where $G = (1/N) \sum_i X_i O_i$, or the computed group average from the aligned data. Equation (3.14) is solved by using an alternating least-squares algorithm until convergence is reached. Given that the transforms are invertible, the original timeseries data and overall connectivity structure for each subject are preserved. See Akrami et al. (2019) for full details. We compute a synchronized group average template from the healthy control subjects with convergence criterion = 1e-6 as in Akrami et al. (2019) and align all subjects to the template.

The ground truth graph for testing between-group differences on subgraphs of features is based on the Glasser cortical parcellation atlas (Glasser et al., 2016) and FreeSurfer's sub-cortical parcels. The graph comprises 23 fully-connected subgraphs, where each subgraph corresponds to a network in the parcellation atlas and is undirected and unweighted. Using window size = 125 TRs and stride = 5 TRs, covariance matrices are estimated from successive, overlapping windows in the timeseries from which we compute covariance trajectories for each subject. For the *fit-of-fits* component, the hyperwindow size = 5.

We test individual subgraphs of features to identify group-level differences in functional connectivity patterns. For each subgraph, we fit both a linear regression model for the subject-specific means and manifold regression model for the subject-specific covariance matrices over time in both groups. We then perform permutation testing by computing the Karcher mean of the covariance trajectories for all subjects in a given group with 1,000 permutations and $\alpha = 0.05$. Experiments are conducted on a computing cluster, in which each

Table 3.3: Networks exhibiting significant group differences from the baseline sFC and dFC methods.

Functional Connectivity	Brain Network	% Regions Found	
		t -stat threshold = 1.66	t -stat threshold = 2.0
sFC	Inferior Parietal Cortex	95%	85%
	Lateral Temporal Cortex	94%	67%
	Dorsolateral Prefrontal Cortex	85%	54%
	Anterior Cingulate and Medial Prefrontal Cortex	87%	80%
	Orbital and Polar Frontal Cortex	82%	64%
	Insular and Frontal Opercular Cortex	77%	50%
	Posterior Cingulate Cortex	75%	50%
	Inferior Frontal Cortex	68%	63%
	Auditory Association Cortex	56%	44%
dFC	Dorsolateral Prefrontal Cortex	65%	
	Anterior Cingulate and Medial Prefrontal Cortex	63%	No
	Orbital and Polar Frontal Cortex	63%	Significant
	Insular and Frontal Opercular Cortex	57%	Regions
	Inferior Frontal Cortex	68%	Identified
	Medial Temporal Cortex	57%	

node consists of Intel Xeon CPU E5-2670 2.6 GHz processors with 32 cores and 256GB RAM. Experiments using the proposed framework are implemented in MATLAB with parallel computing and results are visualized using hcp-utils: <https://github.com/rmldj/hcp-utils>.

3.3.4 Altered connectivity findings from baseline experiments

Using sFC with t -stat threshold = 1.66, 9 networks and 6223 connections were found to be significantly different between patients and healthy controls ($p = 0.005$). We see a considerable reduction in group differences identified with threshold = 2.0, with statistical differences found in 3472 connections ($p = 0.0028$). This indicates that the primary threshold impacts the sensitivity of NBS, given variable results with just two threshold choices. Overall, the large number of group differences identified indicates that the effects of disease are exhibited in distributed impairments within and across networks.

From sliding window analysis of dFC, we identify significant group-level differences in connections across six brain networks ($p = 0.0024$), five of which are consistent with results

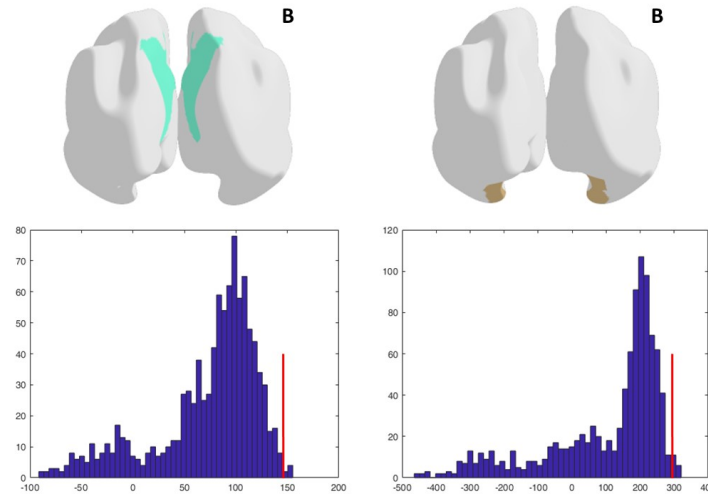


Figure 3.4: Results from baseline scan statistics method with the corresponding estimated null distribution and alternative statistic. (Left) Posterior Cingulate Cortex, (Right) Medial Temporal Cortex. B - visualization from back.

from sFC. In accounting for temporal variability in connectivity, we observe fewer group differences at the connection- and network-level as compared to sFC, suggesting that incorporating temporal dynamics allows for more sensitive assessment of aberrant spatiotemporal patterns. In addition, group differences emerge in connectivity within the Medial Temporal Cortex, which is part of the well-characterized epileptogenic network in TLE (Centeno and Carmichael, 2014). However, we note that experiments run with a t -stat threshold = 2.0 result in no significant group differences identified. Nonetheless, these findings underscore the importance of accounting for the temporal dynamics in connectivity, as it reveals alterations that would otherwise be averaged out. Networks identified in both sets of experiments are listed in Table 3.3.

In representing functional connectivity as SPD matrices on the manifold and comparing pairwise connections, group differences emerge in 4,368 connections. However, after correcting for multiple comparisons, no connections survive the significance threshold. This is not surprising given the large number of multiple comparisons performed on thousands of brain connectivity features. Even in using what is considered to be a more “liberal” multiple test procedure relative to the Bonferroni correction, this approach does not yield any significant

group-level differences.

As shown in Figure 3.4, scan statistics on the full covariance matrices yielded significant group-level differences in two networks found in the baseline sFC and dFC methods. Recall that scan statistics tests the network in its entirety when assessing group differences, whereas NBS only tests sets of connected components that exceed a threshold. Here, we can conclude that when incorporating statistical dependencies between intra-network connections, alterations in groups of functional interactions are evident in both the Posterior Cingulate Cortex and Medial Temporal Cortex in TLE.

3.3.5 Networks identified using covariance trajectory analysis

We evaluate the proposed framework on rs-fMRI data from TLE patients and healthy controls. As shown in Figure 3.5, our method identifies significant between-group differences in the Insular Frontal Opercular Cortex, Inferior Frontal Cortex and Orbital and Polar Frontal Cortex. These networks encompass areas in the default mode network, which has been widely reported to exhibit abnormalities in TLE (McCormick et al., 2013; Zhang et al., 2010a,b). In addition, they comprise regions involved in working memory, a critical function that is known to be impaired in individuals with TLE (Stretton et al., 2014; Stretton and Thompson, 2012). Importantly, our method identified the Subcortical network, which was not discernible using any of the baselines. The Subcortical network includes the hippocampus, thalamus and brainstem, regions commonly within the seizure onset zone or involved in secondary seizure generalization (Morgan et al., 2015; Pittau et al., 2014). We conjecture that these differential effects are appreciable when we go beyond summary measures of correlation or variation and characterize the temporal trajectories of dFC and higher order functional interactions in connectivity. In some cases, the distribution is bimodal with one of the modes below zero, which could be due to a poor group fit from the random sampling of permutations. However, even without these samples, the networks identified would still be statistically significant. Taken together, these results suggest that our framework is capable

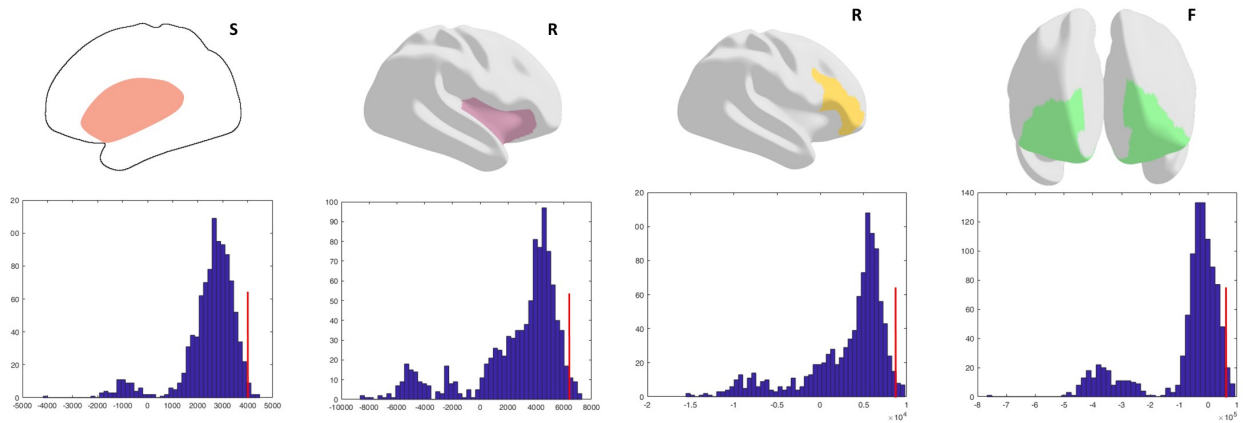


Figure 3.5: Networks exhibiting significant first- and second-order group differences using the proposed method with the corresponding estimated null distribution and alternative statistic: (from left to right) Subcortical, Insular and Frontal Opercular Cortex, Inferior Frontal Cortex, Orbital and Polar Frontal Cortex. S - sagittal view, R - visualization from the right, F - visualization from the front.

of identifying altered brain networks consistent with other methods, but also discovers novel network-wide abnormalities in TLE.

3.4 Discussion and Conclusion

In this work, we present a new application of covariance trajectory analysis to rs-fMRI data to identify brain networks affected in TLE. The proposed method jointly models temporal and functional dependencies in dFC as covariance trajectories on the manifold. Compared to existing brain network modeling frameworks, we show that our method provides an efficient approach to search over and localize discriminative subsets of dFC interactions that stratify TLE patients and controls in a statistically robust manner. As seen from the results, the proposed method detects network-scale disruptions characteristic of TLE, demonstrating the effectiveness of this framework for systems-level characterization of brain function and organization in disease.

In fMRI-based studies, we often encounter high-dimensional, low sample size brain imaging data, which inherently introduces a number of statistical challenges. We demonstrate

that, in performing hypothesis testing on subsets of features rather than thousands of individual connections, the proposed framework can identify statistical differences that do not survive multiple comparison corrections or subjective thresholds common with many existing approaches. In addition, it resolves issues of overestimating significant differences that invariably arise with limited sample sizes, improving sensitivity and generalizability of results. These algorithmic capabilities are critical for exploratory analyses and to probe the manifestations of brain disease on higher order functional interactions across distributed networks in a statistically rigorous manner.

Moreover, Riemannian manifold-based frameworks provide the advantage to utilize the full rsFC covariance matrices for statistical inference. Features in covariance matrices are inherently inter-correlated both mathematically and in the context of functional network organization, therefore, we should leverage these properties to fit more effective brain network models. Few other works have characterized functional connectivity as trajectories on the manifold (Dai et al., 2019; Zhao et al., 2018), however, this work provides a unique *fit-of-fits* solution to perform group analysis on the trajectories that retains spatial and temporal dependencies. This facilitates direct interpretation of discriminative functional interactions between patients and controls that can be compared and validated with the literature.

Provided there exists a conditional independence graph, future work could extend this framework to other neurological diseases or discern structural and functional connectivity as multimodal neuroimaging biomarkers for diagnosis and treatment. In addition, data-driven conditional independence graphs could be used to identify key sub-networks that are altered in network disorders. The framework also offers flexibility to include covariates in a similar construction as Kim et al. (2017), broadening the scope and utility of the proposed method. Other extensions of this framework would be to assess functional brain network dynamics in a longitudinal setting to investigate disease progression. Given the results and benefits offered by our method, the proposed framework holds considerable promise as an fMRI network inference model for investigating altered brain organization and dynamics in disease.

Chapter 4

Characterizing the Alzheimer's Disease Connectome via Differential Covariance Analysis

A.M. Sinha, R. Mehta, V. Nair, G. Hwang, R. Birn, V. Singh, V. Prabhakaran. Investigating functional brain network abnormalities via differential covariance trajectory analysis and scan statistics. *Submitted to ISBI 2022.*

4.1 Introduction

Alzheimer’s Disease (AD) is a neurodegenerative disease known to be the most common cause of dementia among older individuals, accounting for approximately 60-80% of the cases overall (Alzheimer’s & Dementia, 2020). AD causes disruptions in connectivity dynamics across distributed brain networks, and resting-state functional magnetic resonance imaging (rs-fMRI) has shown considerable promise as a tool to capture the functional impairments and discern biomarkers of disease. With the growing evidence of complex spatiotemporal dynamics in dFC and integrated nature of systems in the brain, it is crucial that we account for the temporal dynamics and coordinated interactions between regions when modeling and characterizing functional connectivity in health and disease.

A large number of fMRI studies rely on mass univariate hypothesis testing to perform group comparisons, resolving statistical differences at the connection-level. In the high-dimensional low-sample size data setting that we often encounter in neuroimaging analyses, this approach can be prone to overestimating significant differences or failing to detect differences due to stringent multiple comparisons corrections and/or poor effect sizes. Furthermore, it does not account for functional interactions among groups of regions, or statistical dependencies between connections (features), which underlie normal brain function and the manifestations of disease.

In this paper, we present a pipeline shown in Figure 4.1 that (1) utilizes scan statistics to efficiently search over various subsets of connectivity features, (2) models dFC as temporal trajectories by fitting manifold regressions on the empirical covariance matrices for both groups and (3) performs hypothesis testing to identify subsets of first- and second order differences as biomarkers that distinguish individuals with AD from healthy control subjects.

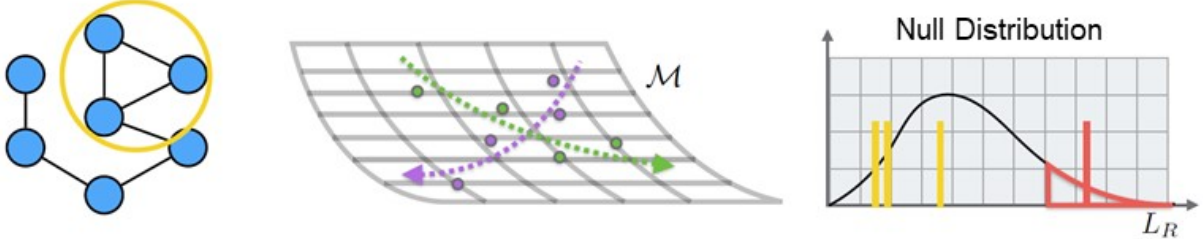


Figure 4.1: The pipeline involves: (1) selecting a subset of features, (2) fitting manifold regressions on empirical covariances for both groups (green and purple) and (3) constructing the likelihood ratio statistic and comparing it against the null distribution via permutation testing.

4.2 Methods

4.2.1 Scan statistics: a multiple testing procedure

In the group difference hypothesis testing problem, we aim to answer the following: are models fit on two groups are the same or significantly different? This can be formulated as a hypothesis test for each structured subgroup R of all subgroups of features \mathcal{R} , if any, that specifically demonstrate this difference in model θ :

$$H_0 : \forall R, \theta_1^R = \theta_2^R \quad vs. \quad H_A : \exists R, \theta_1^R \neq \theta_2^R \quad (4.1)$$

In the absence of *a priori* knowledge of how subgroups of features are formed, testing each subgroup individually would require $2^{|\mathcal{R}|}$ number of tests and a stringent multiple testing correction, with likely few if any features surviving the correction. Recently, Mehta et al. (2019) leveraged concepts from scan statistics to demonstrate that we in fact only need to search over a polynomial number of *structured subgroups* of features. Furthermore, with a specific likelihood ratio statistic and a suitable size correction, an alternative correction can be made based on the subgroup size to circumvent the need for a correction to control the family-wise error rate (FWER).

Consider a graph $\mathcal{G} := (\mathcal{V}, \mathcal{E})$ with a set of vertices or nodes \mathcal{V} and undirected and unweighted edges \mathcal{E} . In the graph, we can define functional networks, which are our subgroups

of features, as fully connected subgraphs. This is our input graph for hypothesis testing on subgroups of features and can be represented as an adjacency matrix, where $(i, j) = 1$ if a pair of ROIs belong to the same network, 0 otherwise.

For subjects $i \in \{1, \dots, N\}$ in a given group (G_1, G_2) , we can calculate a general likelihood ratio statistic for a given R as:

$$L_R = \frac{\prod_{i \in G_1} P(X_i | \theta^1) \prod_{i \in G_2} P(X_i | \theta^2)}{\prod_{i=1}^n P(X_i | \theta)} \quad (4.2)$$

that incorporates dependence over time t , where:

$$P(X_i | \theta) = \prod_{t=1}^T P(X_{i,t} | \mu_t, \Sigma_t) \quad (4.3)$$

We can then compute an alternative correction derived from scan statistics to test against a single null distribution that controls the FWER:

$$T_R = L_R - 2 \sqrt{\log \frac{|E|}{|E(R)|}} \quad (4.4)$$

where $|E|$ is the number of edges (connections) in the full input graph over all networks, and $|E(R)|$ is the number of edges within the subgraph consisting of only subgroup R .

4.2.2 Modeling covariance trajectories

We can model the mean differences in the data μ_t in the above statistic in a straightforward manner: a standard linear model is fit to the data over time t , and the mean μ_t is defined as the predicted average value at each time point, $\mu_t = \beta t$. With high-dimensional, low-sample size data, it is often the case that an empirical covariance computed over all subjects at time t , $\Sigma_t = \hat{\Sigma}_t$, may be rank-deficient. Calculating a multivariate Gaussian likelihood would not be feasible, as it would require inverting the covariance matrix, which is singular.

To resolve this, we can instead *project* the empirical covariance matrices to the symmetric positive definite (SPD) manifold at each time point and fit a regression model to the empirical covariances. As described in Kim et al. (2014); Mehta et al. (2019), we can find a *base point* b and *tangent vector* V that best fits the empirical covariances σ_t to predict the most probable true population covariance at each time point. We can do this by solving the following:

$$\min_{b,V} \frac{1}{2} \sum_{i=1}^n d(\text{Exp}(b, Vt), \sigma_t)^2 \quad (4.5)$$

where $\text{Exp}(\cdot, \cdot)$ represents the exponential map from the tangent space to the SPD manifold, and $d(\cdot, \cdot)$ is the geodesic distance between the fit and the empirical covariance. This is analogous to least squares regression for Euclidean models. The final estimator is then $\Sigma_t = \text{Exp}(b, Vt)$.

4.2.3 Data and Experiments

MRI scans from 27 individuals with Alzheimer’s Disease (14 females, age = 73.7 ± 9.7) and 31 healthy control subjects (15 females, age = 71.9 ± 6.1) were obtained from the Alzheimer’s Disease Connectome Project (ADCP), a multi-site project between the University of Wisconsin-Madison and the Medical College of Wisconsin. Groups were matched with respect to age, gender and education ($p > 0.40$).

MRI data were collected on a 3T GE 750 MRI scanner using a 32-channel head coil. T1-weighted images were acquired using a magnetization prepared gradient echo sequence: TR/TE = 604 ms/2.516 ms, TI = 1060 ms, flip angle = 8° , FOV = 25.6 cm, 0.8 mm isotropic. Rs-fMRI data were acquired using whole-brain simultaneous multi-slice imaging: 8 bands, 72 slices, TR/TE = 802 ms/33.5 ms, flip angle = 50° , FOV = 20.8 cm, 2 mm isotropic voxels.

Data were preprocessed using the Human Connectome Project (HCP) minimal preprocessing pipeline (Glasser et al., 2013) and AFNI (Cox, 1996) to remove spatial distortions, realign volumes to compensate for subject motion, register fMRI to structural data, reduce

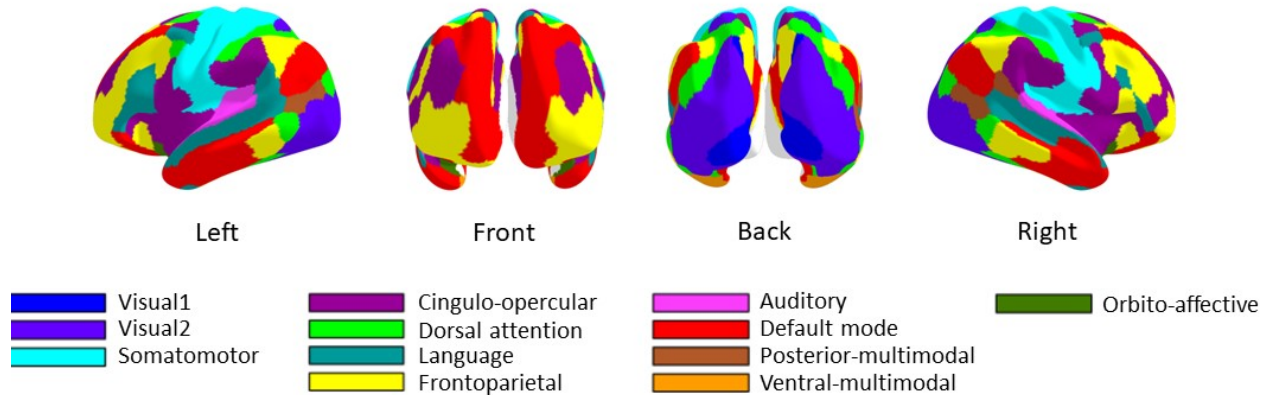


Figure 4.2: 360 parcels in their respective functional brain network based on Ji et al. (2019).

the bias field, normalize the 4D image to a global mean, mask with a final brain mask, perform motion regression using 12 parameters, regress out signal in white matter and cerebrospinal fluid and band-pass filter (0.01 - 0.1 Hz). Two scans acquired with opposite phase encoding directions in the same session were preprocessed separately, normalized and concatenated, resulting in 10 minutes and 40 seconds of scan data (800 TRs) for each subject. The blood oxygen level-dependent (BOLD) timeseries were extracted from $P = 360$ cortical parcels from HCP’s Glasser parcellation (Glasser et al., 2016). Parcels were grouped into their respective functional brain network from the Cole-Anticevic Brain-wide Network Partition (Ji et al., 2019), which comprises 12 networks illustrated in Figure 4.2.

We first employed the conventional static functional connectivity (sFC) and dFC modeling frameworks to compare with our pipeline. We estimated sFC by computing a $P \times P$ connectivity matrix for each subject, where each (i, j) corresponds to the Pearson correlation coefficient between the average timeseries for each pair of parcels, which were transformed into z-score matrices. We estimated dFC by computing correlation between the timeseries of all parcels using the sliding window method with fixed window size = 125 TRs and stride = 5 TRs. Temporal variability in connectivity was computed via standard deviation element-wise across the set of matrices to generate a $P \times P$ dFC matrix for each subject. Group comparisons of sFC and dFC were performed using Network-based statistic (NBS) (Zalesky et al., 2010), a popular statistical method for network-level analysis in fMRI, using

a t -statistic threshold = 1.66 and two-sample t -test (5000 permutations, $p < 0.05$). We considered a network to be significantly different between groups if >50% of unique regions in a network were identified in components of connections exhibiting statistical differences using NBS.

For our pipeline, we utilized the BrainSync Alignment method (Akrami et al., 2019) to temporally align timeseries data across individuals. This ensured that data were aligned in space and time to fit covariance trajectories at the subject- and group-level in a manner that preserves individual differences in connectivity. We computed a synchronized average template from the healthy control subjects with convergence criterion = $1e-6$ and aligned all subjects to the template.

The input graph for hypothesis testing was based on the Cole-Anticevic Brain-wide Network Partition (Ji et al., 2019) and consisted of 12 fully-connected subgraphs. We estimated covariance matrices using the sliding window method with the same parameters as above to fit covariance trajectories for each subject. For each subgraph, we fit a linear regression model and manifold regression model for the subject-level means and covariance matrices, respectively, over time in both groups. Permutation testing was performed by computing the Karcher mean of the covariance trajectories for all subjects in a given group (1000 permutations, $\alpha = 0.05$).

4.3 Results

4.3.1 Altered connectivity findings from baseline experiments

In modeling sFC, significant group differences were detected in 4648 connections across 10 networks ($p = 0.0192$) with >80% regions involved in connections in the Orbito-affective, Auditory, Default mode and Cingulo-opercular networks. Sliding window analysis of dFC revealed 2508 connections exhibiting significant group-level differences ($p = 0.0150$) in AD as compared with healthy controls, including the Frontoparietal, Language, Default mode and

Table 4.1: Networks exhibiting significant group differences from sFC and dFC analyses.

Functional connectivity	Brain network	Total number of regions	% Unique regions found
sFC	Somatomotor	39	51%
	Dorsal-attention	23	65%
	Visual1	6	67%
	Visual2	54	69%
	Frontoparietal	50	76%
	Language	23	78%
	Orbito-affective	6	83%
	Auditory	15	87%
	Default mode	77	99%
	Cingulo-opercular	56	100%
dFC	Frontoparietal	50	62%
	Language	23	65%
	Default mode	77	97%
	Cingulo-opercular	56	98%

Cingulo-opercular networks. Given the consensus that rsFC fluctuates over time, this may indicate going beyond time averaged connectivity to incorporate temporal variability can uncover networks exhibiting pronounced dynamic brain changes. Functional networks comprising connections identified to be significantly different between AD and healthy controls are summarized in Table 4.1.

4.3.2 Altered functional brain networks identified using new pipeline

Experiments using our pipeline yielded significant group differences in three functional networks as shown in Figure 4.3. The somatomotor network is involved in episodic memory, action recognition and spatial navigation, and evidence from previous work have shown that dysfunction of the network is an early sign of AD and worsens with disease progression (Wang et al., 2015). We also identified the frontoparietal network, which plays a crucial role in executive control functioning and has been reported to exhibit significant reductions in within-network connectivity, as well as in interactions with the Default mode network (Zhao

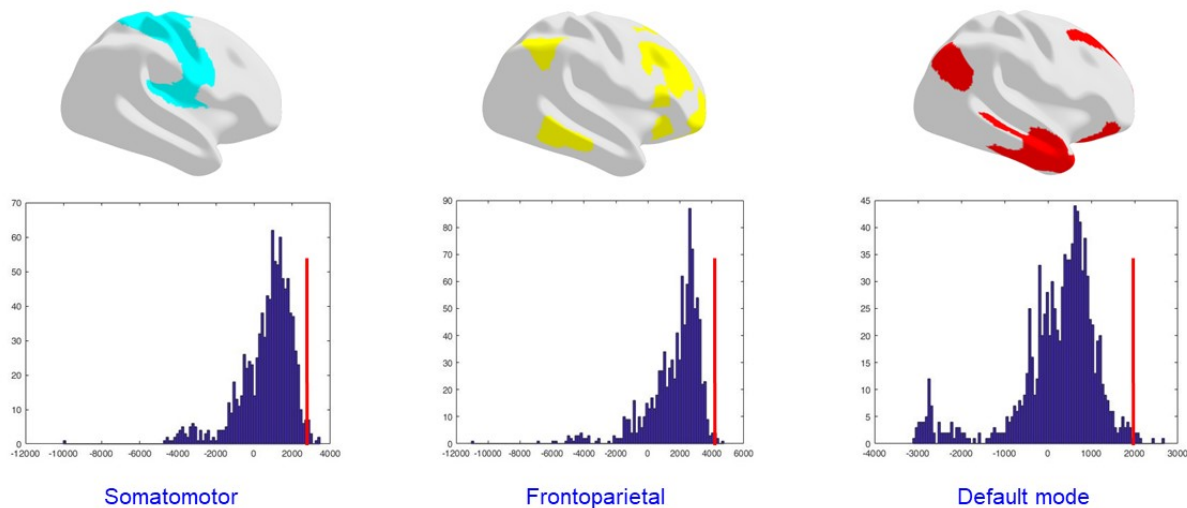


Figure 4.3: Functional networks exhibiting significant first- and second-order group differences with the corresponding estimated null distribution and alternative statistic (red) using our pipeline (brain visualization from right).

et al., 2019). Significant group differences were also identified in the Default mode network, which comprises regions critical for cognitive processing. This is consistent with previous findings of significantly reduced functional connectivity within the default mode network in AD as compared with healthy aging (Damoiseaux et al., 2012), underscoring the clinical value of hypoconnectivity in this network as an early biomarker of the disease Badhwar et al. (2017). Recall that our pipeline identifies discriminative subgroups of temporally covarying features. Therefore, these results may suggest that in AD, there are large-scale disruptions in the temporal dynamics and coordinated interactions among sets of connections in these three networks.

4.4 Discussion and conclusion

In this work, we presented a pipeline that combines a manifold regression scheme with scan statistics to model and investigate alterations in connectivity dynamics in large-scale functional networks. Our findings demonstrate the potential of this pipeline as an effective method to model brain network dynamics and organization in health and disease and address

common statistical challenges that arise with high dimensional functional brain imaging data on small/medium sample sizes. Future work will focus on exploring discriminative subsets of connectivity features that span multiple brain systems to identify key subnetworks in disease.

Chapter 5

Summary and Future Work

5.0.1 Summary

The work presented in this dissertation aimed to identify key areas for methodological improvements in existing methods for functional connectivity analysis and develop new mathematical frameworks that can enable a more rigorous study of neurological diseases. The methods and their applications demonstrate advances in the field of neuroimaging, with a specific focus on rs-fMRI, and provide tangible ways to improve the applicability and robustness of quantitative tools and methods for modeling brain network dynamics.

In Chapter 2, a traditional modeling framework for functional connectivity analysis was combined with a network-based inference method to determine how an alternative form of neurorehabilitation that uses BCI technology affects larger scale brain changes in motor network patterns and functional outcomes in chronic stroke patients. This work enabled us to glean new and critical insights into the therapeutic utility of BCI intervention and how to optimize the neuromodulatory training to facilitate maximal functional motor recovery for patients in the chronic stage of stroke. Importantly, this study also highlighted key statistical challenges inherent to many brain network modeling frameworks that remain an active and ongoing area of research and laid the foundation for subsequent work.

In chapter 3, a new mathematical framework was developed that combines a manifold regression model with graphical scan statistics to model the spatiotemporal patterns of functional connectivity as trajectories on the manifold and localize first- and second-order differences in brain networks affected in TLE. Although manifold-based approaches for fMRI remain a nascent area within the field of fMRI, this work underscored the advantages of performing functional connectivity analysis on the SPD manifold. Furthermore, a *fit-of-fits* construction was implemented to efficiently fit and compare trajectories at both the subject- and group-level to facilitate analysis on high-dimensional rs-fMRI data with respect to sample size, number of features to account for and number of time points. Notably, experimental results demonstrated the effectiveness of scan statistics as a search localization

procedure that can overcome challenges commonly encountered with hypothesis testing in fMRI studies in a statistically rigorous manner with clear interpretability. Moreover, its algorithmic capabilities are particularly useful for exploratory analysis and can enable deeper investigation of brain network organization and the complex mechanisms and widespread impact of disease.

Chapter 4 described the application of the framework developed in the previous chapter to characterize large-scale functional brain network abnormalities in AD. For modeling frameworks to be useful and reliable for studying brain diseases, they must generalize well across age groups, clinical populations and sample sizes. Therefore, the method was evaluated on a much older clinical population, disease process in which there is no lateralization and considerably smaller sample size as compared to previous work. This work added to the growing evidence that scan statistics has considerable potential as a valuable tool for group-level analyses of functional network dynamics to study brain disorders, as it can go beyond individual connections and localize distinct subsets of features, or groups of functional interactions, that exhibit differential signal and may be promising biomarkers of disease. Results showed that the new framework is capable of identifying temporally covarying sets of connectivity features in functional brain networks altered in AD. These findings further suggest that the framework is particularly well suited for neuroimaging studies, which commonly involve data where the sample size is small to medium and comprises high dimensional features with spatial and temporal dependencies.

5.0.2 Future work

In this dissertation, we identified and addressed many methodological and statistical challenges in brain network analysis frameworks to systematically model the spatiotemporal patterns underlying functional network organization. Moreover, we demonstrated the effectiveness of new mathematical frameworks and tools to improve generalizability and reproducibility in functional neuroimaging studies. The work presented here provides new

opportunities to build upon and refine these methodologies to further our understanding of brain connectivity dynamics and organization in health and disease.

In order to further validate the utility of the methods developed here, future work could directly extend these frameworks to other clinical populations and across varying sample sizes. Given that scan statistics has been shown to be an effective tool for group difference testing in settings where the effect size may be poor, it would be of particular importance to determine if it can identify subtle differential effects across the clinical spectrum of a disease. This would provide valuable insight into early signs or biomarkers prior to the early onset of symptoms, as well as elucidate brain changes associated with varying stages of a disease.

Moreover, the work presented here specifically focused on employing the joint manifold regression and scan statistics framework for localizing group differences in intra-network connectivity. A natural extension of the methodology would be to explore and localize discriminative subsets of functional interactions between brain networks, or subnetworks, that could be indicative of underlying brain changes or compensatory mechanisms in healthy brain functioning or disease (Bahrami et al., 2019; Zhu et al., 2019). Furthermore, the mathematical framework developed to model connectivity patterns as temporal trajectories on the manifold characterized large-scale dFC trajectories within the typical rs-fMRI frequency bandwidth. Another potential extension would be to apply the framework to characterize trajectories in narrower fMRI frequency bands, such as slow-5 (0.01–0.027 Hz) and slow-4 (0.027–0.073 Hz) (Buzsáki and Draguhn, 2004), which have been posited to reflect changes in the hemodynamic signals from the gray matter (Zuo et al., 2010). Previous work demonstrated that functional integration among brain regions at "rest" occurs across multiple frequency bands (Gohel and Biswal, 2015) and that features from the lower frequency ranges can elucidate differential patterns in connectivity dynamics (Zhang et al., 2020) and improve classification performance of traditional machine learning models (Hwang et al., 2019b). Therefore, characterizing the temporal trajectories of connectivity patterns in the Slow-5 and Slow-4 bands could uncover functional brain abnormalities in localized subsets

of regions and networks that may only be discernible at lower frequencies.

Most existing fMRI-based studies have used the term "trajectory" to model longitudinal changes in functional connectivity over time. This framework could be extended to investigate changes in functional brain network dynamics in a longitudinal setting to monitor the "trajectory" or progression of disease. Moreover, coupling fMRI data with structural modalities could yield critical insights into the evolving structure-function abnormalities related to disease processes (Sui et al., 2014). Given the benefits offered by scan statistics to efficiently search over and assess group differences on a large number of features, along with the MRI data, demographic characteristics and neuropsychological measures could be incorporated into a multimodal pipeline to facilitate longitudinal analysis in a comprehensive manner. This integrative approach would afford the ability to pinpoint changes in distinct interactions between clinical and neuroimaging features that could explain neurological and cognitive impairments associated with disease.

As a final consideration, it would be important to evaluate the effects of data post-processing on the temporal trajectories of dFC and resulting group differences identified. In capturing the dynamics of functional connectivity, there has been considerable work done to investigate the stability of functional connectivity with respect to scan length (Birn et al., 2013). For example, the effect of varying lengths of fMRI timecourses has been previously investigated in the context of fMRI fingerprinting (Chen et al., 2009). Therefore, it would be of interest to investigate how scan length may affect the stability of group differences identified based on the temporal trajectories of the covariance matrices. In addition, given that temporal alignment was applied to rs-fMRI using an "average healthy controls" template to align subjects in space and time, it would be of interest to determine if and how the subject-level timeseries data and group differences identified are affected if an average template was computed from all subjects in the cohort and subsequent alignment was performed. When temporal ordering is necessary to account for in characterizing the underlying dynamics in rs-fMRI, this will enable us to better understand which dataset should be used as a reference

for alignment of the timeseries data.

In conclusion, the work presented in this dissertation opens to the door to a wide array of future extensions and refinements to build upon the applications and methodologies described here. As the field continues to grow and advance with interdisciplinary efforts across engineering, mathematics and neuroscience, we can continue to develop new and more robust statistical methods, models and tools for rs-fMRI analysis to interrogate and characterize the complex mechanisms and organization of brain function and disease.

Bibliography

- Akrami, H., Joshi, A.A., Li, J., Leahy, R.M., 2019. Group-wise alignment of resting fmri in space and time, in: Medical Imaging 2019: Image Processing, International Society for Optics and Photonics. p. 109492W.
- Allen, E.A., Damaraju, E., Plis, S.M., Erhardt, E.B., Eichele, T., Calhoun, V.D., 2014. Tracking whole-brain connectivity dynamics in the resting state. *Cerebral Cortex* 24, 663–676.
- Ang, K.K., Chua, K.S.G., Phua, K.S., Wang, C., Chin, Z.Y., Kuah, C.W.K., Low, W., Guan, C., 2015. A randomized controlled trial of eeg-based motor imagery brain-computer interface robotic rehabilitation for stroke. *Clinical EEG and Neuroscience* 46, 310–320.
- Arias-Castro, E., Candes, E.J., Durand, A., 2011. Detection of an anomalous cluster in a network. *The Annals of Statistics* , 278–304.
- Arsigny, V., Fillard, P., Pennec, X., Ayache, N., 2006. Log-euclidean metrics for fast and simple calculus on diffusion tensors. *Magnetic Resonance in Medicine* 56, 411–421.
- Badhwar, A., Tam, A., Dansereau, C., Orban, P., Hoffstaedter, F., Bellec, P., 2017. Resting-state network dysfunction in Alzheimer’s Disease: a systematic review and meta-analysis. *Alzheimer’s & Dementia: Diagnosis, Assessment & Disease Monitoring* 8, 73–85.
- Bahrami, M., Laurienti, P.J., Simpson, S.L., 2019. Analysis of brain subnetworks within the context of their whole-brain networks. *Human Brain Mapping* 40, 5123–5141.

- Bajaj, S., Butler, A.J., Drake, D., Dhamala, M., 2015. Brain effective connectivity during motor-imagery and execution following stroke and rehabilitation. *NeuroImage: Clinical* 8, 572–582.
- Baker, J.T., Holmes, A.J., Masters, G.A., Yeo, B.T., Krienen, F., Buckner, R.L., Öngür, D., 2014. Disruption of cortical association networks in schizophrenia and psychotic bipolar disorder. *JAMA Psychiatry* 71, 109–118.
- Ballester, B.R., Maier, M., Mozo, R.M.S.S., Castañeda, V., Duff, A., Verschure, P.F., 2016. Counteracting learned non-use in chronic stroke patients with reinforcement-induced movement therapy. *Journal of Neuroengineering and Rehabilitation* 13, 1–15.
- Banerjee, M., Chakraborty, R., Ofori, E., Vaillancourt, D., Vemuri, B.C., 2015. Nonlinear regression on riemannian manifolds and its applications to neuro-image analysis, in: *International Conference on Medical Image Computing and Computer-Assisted Intervention*, Springer. pp. 719–727.
- Benjamin, E.J., Blaha, M.J., Chiuve, S.E., Cushman, M., Das, S.R., Deo, R., De Ferranti, S.D., Floyd, J., Fornage, M., Gillespie, C., et al., 2017. Heart Disease and Stroke Statistics—2017 Update: A Report From the American Heart Association. *Circulation* 135, e146–e603.
- Benjamini, Y., Hochberg, Y., 1995. Controlling the false discovery rate: a practical and powerful approach to multiple testing. *Journal of the Royal Statistical Society: series B (Methodological)* 57, 289–300.
- Betzell, R.F., Bassett, D.S., 2017. Multi-scale brain networks. *NeuroImage* 160, 73–83.
- Betzell, R.F., Fukushima, M., He, Y., Zuo, X.N., Sporns, O., 2016. Dynamic fluctuations coincide with periods of high and low modularity in resting-state functional brain networks. *NeuroImage* 127, 287–297.

- Biasiucci, A., Leeb, R., Iturrate, I., Perdakis, S., Al-Khodairy, A., Corbet, T., Schnider, A., Schmidlin, T., Zhang, H., Bassolino, M., et al., 2018. Brain-actuated functional electrical stimulation elicits lasting arm motor recovery after stroke. *Nature Communications* 9, 1–13.
- Birbeck, G.L., 2010. Epilepsy care in developing countries: part i of ii. *Epilepsy Currents* 10, 75–79.
- Birn, R.M., Molloy, E.K., Patriat, R., Parker, T., Meier, T.B., Kirk, G.R., Nair, V.A., Meyerand, M.E., Prabhakaran, V., 2013. The effect of scan length on the reliability of resting-state fMRI connectivity estimates. *NeuroImage* 83, 550–558.
- Biswal, B., Zerrin Yetkin, F., Haughton, V.M., Hyde, J.S., 1995. Functional connectivity in the motor cortex of resting human brain using echo-planar MRI. *Magnetic Resonance in Medicine* 34, 537–541.
- Brauer, S.G., Hayward, K.S., Carson, R.G., Cresswell, A.G., Barker, R.N., 2013. The efficacy of SMART Arm training early after stroke for stroke survivors with severe upper limb disability: a protocol for a randomised controlled trial. *BMC Neurology* 13, 1–8.
- Broetz, D., Braun, C., Weber, C., Soekadar, S.R., Caria, A., Birbaumer, N., 2010. Combination of brain-computer interface training and goal-directed physical therapy in chronic stroke: a case report. *Neurorehabilitation and Neural Repair* 24, 674–679.
- Buetefisch, C.M., 2015. Role of the contralesional hemisphere in post-stroke recovery of upper extremity motor function. *Frontiers in Neurology* 6, 214.
- Bundy, D.T., Souders, L., Baranyai, K., Leonard, L., Schalk, G., Coker, R., Moran, D.W., Huskey, T., Leuthardt, E.C., 2017. Contralesional brain-computer interface control of a powered exoskeleton for motor recovery in chronic stroke survivors. *Stroke* 48, 1908–1915.

- Buzsáki, G., Draguhn, A., 2004. Neuronal oscillations in cortical networks. *Science* 304, 1926–1929.
- Calhoun, V.D., Kiehl, K.A., Pearlson, G.D., 2008. Modulation of temporally coherent brain networks estimated using ICA at rest and during cognitive tasks. *Human Brain Mapping* 29, 828–838.
- Calhoun, V.D., Miller, R., Pearlson, G., Adalı, T., 2014. The chronnectome: time-varying connectivity networks as the next frontier in fMRI data discovery. *Neuron* 84, 262–274.
- Carod-Artal, F.J., Coral, L.F., Trizotto, D.S., Moreira, C.M., 2008. The Stroke Impact Scale 3.0: evaluation of acceptability, reliability, and validity of the Brazilian version. *Stroke* 39, 2477–2484.
- Carroll, D., 1965. A quantitative test of upper extremity function. *Journal of Chronic Diseases* 18, 479–491.
- Carter, A.R., Connor, L.T., Dromerick, A.W., 2010. Rehabilitation after stroke: current state of the science. *Current Neurology and Neuroscience Reports* 10, 158–166.
- Celebi, M.E., Kingravi, H.A., Vela, P.A., 2013. A comparative study of efficient initialization methods for the k-means clustering algorithm. *Expert Systems with Applications* 40, 200–210.
- Centeno, M., Carmichael, D.W., 2014. Network connectivity in epilepsy: resting state fMRI and EEG–fMRI contributions. *Frontiers in Neurology* 5, 93.
- Chang, C., Glover, G.H., 2010. Time–frequency dynamics of resting-state brain connectivity measured with fMRI. *NeuroImage* 50, 81–98.
- Chen, H.M., Chen, C.C., Hsueh, I.P., Huang, S.L., Hsieh, C.L., 2009. Test-retest reproducibility and smallest real difference of 5 hand function tests in patients with stroke. *Neurorehabilitation and Neural Repair* 23, 435–440.

- Chiang, S., Cassese, A., Guindani, M., Vannucci, M., Yeh, H.J., Haneef, Z., Stern, J.M., 2016. Time-dependence of graph theory metrics in functional connectivity analysis. *NeuroImage* 125, 601–615.
- Cho, W., Heilinger, A., Ortner, R., Murovec, N., Xu, R., Zehetner, M., Gruenwald, J., Schobesberger, S., Schnuerer, A., Guger, C., 2018. Feasibility of Brain-Computer Interface Triggered Functional Electrical Stimulation and Avatar for Motor Improvement in Chronic Stroke Patients, in: *International Conference on NeuroRehabilitation*, Springer. pp. 1097–1100.
- Cook, C.J., Hwang, G., Mathis, J., Nair, V.A., Conant, L.L., Allen, L., Almane, D.N., Birn, R., DeYoe, E.A., Felton, E., et al., 2019. Effective Connectivity Within the Default Mode Network in Left Temporal Lobe Epilepsy: Findings from the Epilepsy Connectome Project. *Brain Connectivity* 9, 174–183.
- Cornea, E., Zhu, H., Kim, P., Ibrahim, J.G., 2017. Regression models on riemannian symmetric spaces. *Journal of the Royal Statistical Society. Series B, Statistical methodology* 79, 463.
- Cox, R.W., 1996. Afni: software for analysis and visualization of functional magnetic resonance neuroimages. *Computers and Biomedical Research* 29, 162–173.
- Cribben, I., Haraldsdottir, R., Atlas, L.Y., Wager, T.D., Lindquist, M.A., 2012. Dynamic connectivity regression: determining state-related changes in brain connectivity. *NeuroImage* 61, 907–920.
- Cribben, I., Wager, T., Lindquist, M., 2013. Detecting functional connectivity change points for single-subject fMRI data. *Frontiers in Computational Neuroscience* 7, 143.
- Dai, M., Zhang, Z., Srivastava, A., 2019. Analyzing dynamical brain functional connectivity

- as trajectories on space of covariance matrices. *IEEE Transactions on Medical Imaging* 39, 611–620.
- Daly, J.J., Cheng, R., Rogers, J., Litinas, K., Hrovat, K., Dohring, M., 2009. Feasibility of a New Application of Noninvasive Brain Computer Interface (BCI): A Case Study of Training for Recovery of Volitional Motor Control After Stroke. *Journal of Neurologic Physical Therapy* 33, 203–211.
- Damaraju, E., Allen, E.A., Belger, A., Ford, J.M., McEwen, S., Mathalon, D., Mueller, B., Pearlson, G., Potkin, S., Preda, A., et al., 2014. Dynamic functional connectivity analysis reveals transient states of dysconnectivity in Schizophrenia. *NeuroImage: Clinical* 5, 298–308.
- Damoiseaux, J.S., Prater, K.E., Miller, B.L., Greicius, M.D., 2012. Functional connectivity tracks clinical deterioration in Alzheimer’s disease. *Neurobiology of Aging* 33, 828–e19.
- Dimyan, M.A., Cohen, L.G., 2011. Neuroplasticity in the context of motor rehabilitation after stroke. *Nature Reviews Neurology* 7, 76–85.
- Do, A.H., Wang, P.T., King, C.E., Schombs, A., Cramer, S.C., Nenadic, Z., 2012. Brain-computer interface controlled functional electrical stimulation device for foot drop due to stroke, in: *International Conference of the IEEE Engineering in Medicine and Biology Society, IEEE*. pp. 6414–6417.
- Dodd, K.C., Nair, V.A., Prabhakaran, V., 2017. Role of the Contralesional vs. Ipsilesional Hemisphere in Stroke Recovery. *Frontiers in Human Neuroscience* 11, 469.
- Du, J., Goh, A., Kushnarev, S., Qiu, A., 2014. Geodesic regression on orientation distribution functions with its application to an aging study. *NeuroImage* 87, 416–426.
- Du, Y., Fu, Z., Calhoun, V.D., 2018. Classification and prediction of brain disorders using functional connectivity: promising but challenging. *Frontiers in Neuroscience* 12, 525.

- Duncan, P.W., Wallace, D., Lai, S.M., Johnson, D., Embretson, S., Laster, L.J., 1999. The Stroke Impact Scale version 2.0: evaluation of reliability, validity, and sensitivity to change. *Stroke* 30, 2131–2140.
- Fan, Y.t., Wu, C.y., Liu, H.l., Lin, K.c., Wai, Y.y., Chen, Y.l., 2015. Neuroplastic changes in resting-state functional connectivity after stroke rehabilitation. *Frontiers in Human Neuroscience* 9, 546.
- Finn, E.S., Huber, L., Jangraw, D.C., Molfese, P.J., Bandettini, P.A., 2019. Layer-dependent activity in human prefrontal cortex during working memory. *Nature Neuroscience* 22, 1687–1695.
- Fletcher, P.T., 2013. Geodesic Regression and the Theory of Least Squares on Riemannian Manifolds. *International Journal of Computer Vision* 105, 171–185.
- Fletcher, P.T., Joshi, S., 2007. Riemannian geometry for the statistical analysis of diffusion tensor data. *Signal Processing* 87, 250–262.
- Garcia, J.O., Ashourvan, A., Muldoon, S., Vettel, J.M., Bassett, D.S., 2018. Applications of community detection techniques to brain graphs: Algorithmic considerations and implications for neural function. *Proceedings of the IEEE* 106, 846–867.
- Glasser, M.F., Coalson, T.S., Robinson, E.C., Hacker, C.D., Harwell, J., Yacoub, E., Ugurbil, K., Andersson, J., Beckmann, C.F., Jenkinson, M., et al., 2016. A multi-modal parcellation of human cerebral cortex. *Nature* 536, 171.
- Glasser, M.F., Sotiropoulos, S.N., Wilson, J.A., Coalson, T.S., Fischl, B., Andersson, J.L., Xu, J., Jbabdi, S., Webster, M., Polimeni, J.R., et al., 2013. The minimal preprocessing pipelines for the Human Connectome Project. *NeuroImage* 80, 105–124.
- Gohel, S.R., Biswal, B.B., 2015. Functional integration between brain regions at rest occurs in multiple-frequency bands. *Brain Connectivity* 5, 23–34.

- Gordon, E.M., Laumann, T.O., Adeyemo, B., Huckins, J.F., Kelley, W.M., Petersen, S.E., 2016. Generation and evaluation of a cortical area parcellation from resting-state correlations. *Cerebral Cortex* 26, 288–303.
- Grefkes, C., Eickhoff, S.B., Nowak, D.A., Dafotakis, M., Fink, G.R., 2008. Dynamic intra- and interhemispheric interactions during unilateral and bilateral hand movements assessed with fMRI and DCM. *NeuroImage* 41, 1382–1394.
- Hanley, J., Negassa, A., Edwardes, M., Forrester, J., 2003. Statistical Analysis of Correlated Data using Generalized Estimating Equations: An Orientation. *American Journal of Epidemiology* 157, 364–375.
- Hutchison, R.M., Womelsdorf, T., Allen, E.A., Bandettini, P.A., Calhoun, V.D., Corbetta, M., Della Penna, S., Duyn, J.H., Glover, G.H., Gonzalez-Castillo, J., et al., 2013. Dynamic functional connectivity: Promise, issues, and interpretations. *NeuroImage* 80, 360–378.
- Hwang, G., Dabbs, K., Conant, L., Nair, V.A., Mathis, J., Almane, D.N., Nencka, A., Birn, R., Humphries, C., Raghavan, M., et al., 2019a. Cognitive Slowing and Its Underlying Neurobiology in Temporal Lobe Epilepsy. *Cortex* 117, 41–52.
- Hwang, G., Nair, V.A., Mathis, J., Cook, C.J., Mohanty, R., Zhao, G., Tellapragada, N., Ustine, C., Nwoke, O.O., Rivera-Bonet, C., et al., 2019b. Using Low-Frequency Oscillations to Detect Temporal Lobe Epilepsy with Machine Learning. *Brain Connectivity* 9, 184–193.
- Ji, J.L., Spronk, M., Kulkarni, K., Repovš, G., Anticevic, A., Cole, M.W., 2019. Mapping the human brain’s cortical-subcortical functional network organization. *NeuroImage* 185, 35–57.
- Kaczmarek, K.A., 2011. The tongue display unit (TDU) for electrotactile spatiotemporal pattern presentation. *Scientia Iranica* 18, 1476–1485.

- Kang, N., Summers, J.J., Cauraugh, J.H., 2016. Transcranial direct current stimulation facilitates motor learning post-stroke: a systematic review and meta-analysis. *Journal of Neurology, Neurosurgery & Psychiatry* 87, 345–355.
- Karcher, H., 1977. Riemannian center of mass and mollifier smoothing. *Communications on Pure and Applied Mathematics* 30, 509–541.
- Katzan, I.L., Thompson, N.R., Lapin, B., Uchino, K., 2017. Added value of patient-reported outcome measures in stroke clinical practice. *Journal of the American Heart Association* 6, e005356.
- Kim, H.J., Adluru, N., Collins, M.D., Chung, M.K., Bendlin, B.B., Johnson, S.C., Davidson, R.J., Singh, V., 2014. Multivariate General Linear Models (MGLM) on Riemannian Manifolds with Applications to Statistical Analysis of Diffusion Weighted Images, in: *Proceedings of the IEEE Conference on Computer Vision and Pattern Recognition*, pp. 2705–2712.
- Kim, H.J., Adluru, N., Suri, H., Vemuri, B.C., Johnson, S.C., Singh, V., 2017. Riemannian Nonlinear Mixed Effects Models: Analyzing Longitudinal Deformations in Neuroimaging, in: *Proceedings of the IEEE Conference on Computer Vision and Pattern Recognition*, pp. 2540–2549.
- Klugah-Brown, B., Luo, C., He, H., Jiang, S., Armah, G.K., Wu, Y., Li, J., Yin, W., Yao, D., 2019. Altered Dynamic Functional Network Connectivity in Frontal Lobe Epilepsy. *Brain Topography* 32, 394–404.
- Kucyi, A., Davis, K.D., 2014. Dynamic functional connectivity of the default mode network tracks daydreaming. *NeuroImage* 100, 471–480.
- Laird, A.R., Fox, P.M., Eickhoff, S.B., Turner, J.A., Ray, K.L., McKay, D.R., Glahn, D.C.,

- Beckmann, C.F., Smith, S.M., Fox, P.T., 2011. Behavioral interpretations of intrinsic connectivity networks. *Journal of Cognitive Neuroscience* 23, 4022–4037.
- Lang, C.E., Wagner, J.M., Dromerick, A.W., Edwards, D.F., 2006. Measurement of Upper-Extremity Function Early After Stroke: Properties of the Action Research Arm Test. *Archives of Physical Medicine and Rehabilitation* 87, 1605–1610.
- Lang, K.C., Thompson, P.A., Wolf, S.L., 2013. The EXCITE Trial: Reacquiring Upper-Extremity Task Performance With Early Versus Late Delivery of Constraint Therapy. *Neurorehabilitation and Neural Repair* 27, 654–663.
- Lee, J., Park, E., Lee, A., Chang, W.H., Kim, D.S., Kim, Y.H., 2018. Alteration and role of interhemispheric and intrahemispheric connectivity in motor network after stroke. *Brain topography* 31, 708–719.
- Van der Lee, J.H., Wagenaar, R.C., Lankhorst, G.J., Vogelaar, T.W., Devillé, W.L., Bouter, L.M., 1999. Forced Use of the Upper Extremity in Chronic Stroke Patients. *Stroke* 30, 2369–2375.
- Lee, J.M., 2006. *Riemannian Manifolds: An Introduction to Curvature*. volume 176. Springer Science & Business Media.
- Lee, M.H., Smyser, C.D., Shimony, J.S., 2013. Resting-State fMRI: A Review of Methods and Clinical Applications. *American Journal of neuroradiology* 34, 1866–1872.
- Leonardi, N., Richiardi, J., Gschwind, M., Simioni, S., Annoni, J.M., Schlupe, M., Vuilleumier, P., Van De Ville, D., 2013. Principal components of functional connectivity: a new approach to study dynamic brain connectivity during rest. *NeuroImage* 83, 937–950.
- Li, X., Zhu, D., Jiang, X., Jin, C., Zhang, X., Guo, L., Zhang, J., Hu, X., Li, L., Liu, T., 2014. Dynamic functional connectomics signatures for characterization and differentiation of PTSD patients. *Human Brain Mapping* 35, 1761–1778.

- Liu, F., Wang, Y., Li, M., Wang, W., Li, R., Zhang, Z., Lu, G., Chen, H., 2017. Dynamic Functional Network Connectivity in Idiopathic Generalized Epilepsy with Generalized Tonic–Clonic Seizure. *Human Brain Mapping* 38, 957–973.
- Lurie, D.J., Kessler, D., Bassett, D.S., Betzel, R.F., Breakspear, M., Kheilholz, S., Kucyi, A., Liégeois, R., Lindquist, M.A., McIntosh, A.R., et al., 2020. Questions and controversies in the study of time-varying functional connectivity in resting fMRI. *Network Neuroscience* 4, 30–69.
- Mahoney, F.I., Barthel, D.W., 1965. Functional evaluation: The Barthel Index: a simple index of independence useful in scoring improvement in the rehabilitation of the chronically ill. *Maryland State Medical Journal* .
- McCormick, C., Quraan, M., Cohn, M., Valiante, T.A., McAndrews, M.P., 2013. Default mode network connectivity indicates episodic memory capacity in mesial temporal lobe epilepsy. *Epilepsia* 54, 809–818.
- Mehta, R., Kim, H., Wang, S., Johnson, S., Yuan, M., Singh, V., 2019. Localizing differentially evolving covariance structures via scan statistics. *Quarterly of Applied Mathematics* 77, 357–398.
- Menon, R.S., Kim, S.G., 1999. Spatial and temporal limits in cognitive neuroimaging with fMRI. *Trends in Cognitive Sciences* 3, 207–216.
- Michielsen, M.E., Selles, R.W., van der Geest, J.N., Eckhardt, M., Yavuzer, G., Stam, H.J., Smits, M., Ribbers, G.M., Bussmann, J.B., 2011. Motor Recovery and Cortical Reorganization After Mirror Therapy in Chronic Stroke Patients: A Phase II Randomized Controlled Trial. *Neurorehabilitation and Neural Repair* 25, 223–233.
- Min, Y.S., Park, J.W., Park, E., Kim, A.R., Cha, H., Gwak, D.W., Jung, S.H., Chang, Y., Jung, T.D., 2020. Interhemispheric Functional Connectivity in the Primary Motor

- Cortex Assessed by Resting-State Functional Magnetic Resonance Imaging Aids Long-Term Recovery Prediction among Subacute Stroke Patients with Severe Hand Weakness. *Journal of Clinical Medicine* 9, 975.
- Mohanty, R., Sinha, A.M., Remsik, A.B., Dodd, K.C., Young, B.M., Jacobson, T., McMillan, M., Thoma, J., Advani, H., Nair, V.A., et al., 2018. Machine learning classification to identify the stage of brain-computer interface therapy for stroke rehabilitation using functional connectivity. *Frontiers in Neuroscience* 12, 353.
- Morgan, V.L., Abou-Khalil, B., Rogers, B.P., 2015. Evolution of Functional Connectivity of Brain Networks and Their Dynamic Interaction in Temporal Lobe Epilepsy. *Brain Connectivity* 5, 35–44.
- Mukaino, M., Ono, T., Shindo, K., Fujiwara, T., Ota, T., Kimura, A., Liu, M., Ushiba, J., 2014. Efficacy of brain-computer interface-driven neuromuscular electrical stimulation for chronic paresis after stroke. *Journal of Rehabilitation Medicine* 46, 378–382.
- Murase, N., Duque, J., Mazzocchio, R., Cohen, L.G., 2004. Influence of interhemispheric interactions on motor function in chronic stroke. *Annals of Neurology* 55, 400–409.
- Nair, V.A., Young, B.M., Nigogosyan, Z., Remsick, A., Weber, S., Diffie, K., Walton, L., Tyler, M., Sattin, J., Edwards, D.F., et al., 2015. Resting-state Functional Connectivity Changes After Stroke Rehabilitation Using Closed Loop Neurofeedback. *Stroke* 46, A6–A6.
- Ng, B., Varoquaux, G., Poline, J.B., Greicius, M., Thirion, B., 2015. Transport on Riemannian Manifold for Connectivity-Based Brain Decoding. *IEEE Transactions on Medical Imaging* 35, 208–216.
- Oldfield, R.C., 1971. The assessment and analysis of handedness: the edinburgh inventory. *Neuropsychologia* 9, 97–113.

- Omidvarnia, A., Pedersen, M., Walz, J.M., Vaughan, D.N., Abbott, D.F., Jackson, G.D., 2016. Dynamic regional phase synchrony (DRePS): An Instantaneous Measure of Local fMRI Connectivity Within Spatially Clustered Brain Areas. *Human Brain Mapping* 37, 1970–1985.
- Ono, T., Shindo, K., Kawashima, K., Ota, N., Ito, M., Ota, T., Mukaino, M., Fujiwara, T., Kimura, A., Liu, M., et al., 2014. Brain-computer interface with somatosensory feedback improves functional recovery from severe hemiplegia due to chronic stroke. *Frontiers in Neuroengineering* 7, 19.
- Park, Y., Wang, H., Nöbauer, T., Vaziri, A., Priebe, C.E., 2015. Anomaly Detection on Whole-Brain Functional Imaging of Neuronal Activity using Graph Scan Statistics. *Neuron* 2, 4–000.
- Pennec, X., Fillard, P., Ayache, N., 2006. A Riemannian Framework for Tensor Computing. *International Journal of Computer Vision* 66, 41–66.
- Pichiorri, F., Morone, G., Petti, M., Toppi, J., Pisotta, I., Molinari, M., Paolucci, S., Inghilleri, M., Astolfi, L., Cincotti, F., et al., 2015. Brain–computer interface boosts motor imagery practice during stroke recovery. *Annals of Neurology* 77, 851–865.
- Pittau, F., Mégevand, P., Sheybani, L., Abela, E., Grouiller, F., Spinelli, L., Michel, C.M., Seeck, M., Vulliemoz, S., 2014. Mapping Epileptic Activity: Sources or Networks for the Clinicians? *Frontiers in Neurology* 5, 218.
- Power, J.D., Barnes, K.A., Snyder, A.Z., Schlaggar, B.L., Petersen, S.E., 2012. Spurious but systematic correlations in functional connectivity MRI networks arise from subject motion. *NeuroImage* 59, 2142–2154.
- Preti, M.G., Bolton, T.A., Van De Ville, D., 2017. The dynamic functional connectome: State-of-the-art and perspectives. *NeuroImage* 160, 41–54.

- Qiu, A., Lee, A., Tan, M., Chung, M.K., 2015. Manifold learning on brain functional networks in aging. *Medical Image Analysis* 20, 52–60.
- Ramos-Murguialday, A., Curado, M.R., Broetz, D., Yilmaz, Ö., Brasil, F.L., Liberati, G., Garcia-Cossio, E., Cho, W., Caria, A., Cohen, L.G., et al., 2019. Brain-Machine-Interface in Chronic Stroke: Randomised Trial Long-Term Follow-up. *Neurorehabilitation and Neural Repair* 33, 188–198.
- Remsik, A.B., Williams Jr, L., Gjini, K., Dodd, K., Thoma, J., Jacobson, T., Walczak, M., McMillan, M., Rajan, S., Young, B.M., et al., 2019. Ipsilesional Mu Rhythm Desynchronization and Changes in Motor Behavior Following Post Stroke BCI Intervention for Motor Rehabilitation. *Frontiers in Neuroscience* 13, 53.
- Richardson, M., Campbell, N., Allen, L., Meyer, M., Teasell, R., 2016. The stroke impact scale: performance as a quality of life measure in a community-based stroke rehabilitation setting. *Disability and Rehabilitation* 38, 1425–1430.
- Schalk, G., McFarland, D.J., Hinterberger, T., Birbaumer, N., Wolpaw, J.R., 2004. BCI2000: a general-purpose brain-computer interface (BCI) system. *IEEE Transactions on Biomedical Engineering* 51, 1034–1043.
- Schwab, S., Harbord, R., Zerbi, V., Elliott, L., Afyouni, S., Smith, J.Q., Woolrich, M.W., Smith, S.M., Nichols, T.E., 2018. Directed functional connectivity using dynamic graphical models. *NeuroImage* 175, 340–353.
- Shakil, S., Lee, C.H., Keilholz, S.D., 2016. Evaluation of sliding window correlation performance for characterizing dynamic functional connectivity and brain states. *NeuroImage* 133, 111–128.
- Smith, S.M., Fox, P.T., Miller, K.L., Glahn, D.C., Fox, P.M., Mackay, C.E., Filippini, N., Watkins, K.E., Toro, R., Laird, A.R., et al., 2009. Correspondence of the brain’s functional

- architecture during activation and rest. *Proceedings of the National Academy of Sciences* 106, 13040–13045.
- Smith, S.M., Miller, K.L., Moeller, S., Xu, J., Auerbach, E.J., Woolrich, M.W., Beckmann, C.F., Jenkinson, M., Andersson, J., Glasser, M.F., et al., 2012. Temporally-independent functional modes of spontaneous brain activity. *Proceedings of the National Academy of Sciences* 109, 3131–3136.
- Smitha, K., Akhil Raja, K., Arun, K., Rajesh, P., Thomas, B., Kapilamoorthy, T., Kesavadas, C., 2017. Resting state fMRI: A review on methods in resting state connectivity analysis and resting state networks. *The Neuroradiology Journal* 30, 305–317.
- Soekadar, S.R., Birbaumer, N., Slutzky, M.W., Cohen, L.G., 2015. Brain–machine interfaces in neurorehabilitation of stroke. *Neurobiology of Disease* 83, 172–179.
- Song, J., Nair, V.A., Young, B.M., Walton, L.M., Nigogosyan, Z., Remsik, A., Tyler, M.E., Farrar-Edwards, D., Caldera, K.E., Sattin, J.A., et al., 2015. DTI measures track and predict motor function outcomes in stroke rehabilitation utilizing BCI technology. *Frontiers in Human Neuroscience* 9, 195.
- Stagg, C.J., Bachtiar, V., O’Shea, J., Allman, C., Bosnell, R.A., Kischka, U., Matthews, P.M., Johansen-Berg, H., 2012. Cortical activation changes underlying stimulation-induced behavioural gains in chronic stroke. *Brain* 135, 276–284.
- Stewart, J.C., Cramer, S.C., 2013. Patient-reported measures provide unique insights into motor function after stroke. *Stroke* 44, 1111–1116.
- Stretton, J., Sidhu, M.K., Winston, G.P., Bartlett, P., McEvoy, A.W., Symms, M.R., Koepp, M.J., Thompson, P.J., Duncan, J.S., 2014. Working memory network plasticity after anterior temporal lobe resection: a longitudinal functional magnetic resonance imaging study. *Brain* 137, 1439–1453.

- Stretton, J., Thompson, P., 2012. Frontal lobe function in temporal lobe epilepsy. *Epilepsy Research* 98, 1–13.
- Sui, J., Huster, R., Yu, Q., Segall, J.M., Calhoun, V.D., 2014. Function–structure associations of the brain: evidence from multimodal connectivity and covariance studies. *Neuroimage* 102, 11–23.
- Téllez-Zenteno, J.F., Hernández-Ronquillo, L., 2012. A review of the epidemiology of temporal lobe epilepsy. *Epilepsy Research and Treatment* 2012.
- Trujillo, P., Mastropietro, A., Scano, A., Chiavenna, A., Mrakic-Sposta, S., Caimmi, M., Molteni, F., Rizzo, G., 2017. Quantitative EEG for Predicting Upper Limb Motor Recovery in Chronic Stroke Robot-Assisted Rehabilitation. *IEEE Transactions on Neural Systems and Rehabilitation Engineering* 25, 1058–1067.
- Tsuchimoto, S., Shindo, K., Hotta, F., Hanakawa, T., Liu, M., Ushiba, J., 2019. Sensorimotor connectivity after motor exercise with neurofeedback in post-stroke patients with hemiplegia. *Neuroscience* 416, 109–125.
- Urbin, M.A., Hong, X., Lang, C.E., Carter, A.R., 2014. Resting-State Functional Connectivity and Its Association With Multiple Domains of Upper-Extremity Function in Chronic Stroke. *Neurorehabilitation and Neural Repair* 28, 761–769.
- Vahdat, S., Darainy, M., Thiel, A., Ostry, D.J., 2019. A Single Session of Robot-Controlled Proprioceptive Training Modulates Functional Connectivity of Sensory Motor Networks and Improves Reaching Accuracy in Chronic Stroke. *Neurorehabilitation and Neural Repair* 33, 70–81.
- Varkuti, B., Guan, C., Pan, Y., Phua, K.S., Ang, K.K., Kuah, C.W.K., Chua, K., Ang, B.T., Birbaumer, N., Sitaram, R., 2013. Resting State Changes in Functional Connec-

- tivity Correlate With Movement Recovery for BCI and Robot-Assisted Upper-Extremity Training After Stroke. *Neurorehabilitation and Neural Repair* 27, 53–62.
- Varoquaux, G., Baronnet, F., Kleinschmidt, A., Fillard, P., Thirion, B., 2010. Detection of Brain Functional-Connectivity Difference in Post-stroke Patients Using Group-Level Covariance Modeling, in: *International Conference on Medical Image Computing and Computer-Assisted Intervention*, Springer. pp. 200–208.
- Venkatesh, M., Jaja, J., Pessoa, L., 2020. Comparing functional connectivity matrices: A geometry-aware approach applied to participant identification. *NeuroImage* 207, 116398.
- Wang, H., Tang, M., Park, Y., Priebe, C.E., 2013. Locality Statistics for Anomaly Detection in Time Series of Graphs. *IEEE Transactions on Signal Processing* 62, 703–717.
- Wang, P., Zhou, B., Yao, H., Zhan, Y., Zhang, Z., Cui, Y., Xu, K., Ma, J., Wang, L., An, N., et al., 2015. Aberrant intra-and inter-network connectivity architectures in Alzheimer’s Disease and mild cognitive impairment. *Scientific Reports* 5, 1–12.
- Ward, N., Brown, M., Thompson, A., Frackowiak, R., 2003. Neural correlates of motor recovery after stroke: a longitudinal fMRI study. *Brain* 126, 2476–2496.
- Wilson, J.A., Schalk, G., Walton, L.M., Williams, J.C., 2009. Using an EEG-Based Brain-Computer Interface for Virtual Cursor Movement with BCI2000. *Journal of Visualized Experiments* , e1319.
- Wilson, J.A., Walton, L.M., Tyler, M., Williams, J., 2012. Lingual electrotactile stimulation as an alternative sensory feedback pathway for brain–computer interface applications. *Journal of Neural Engineering* 9, 045007.
- Wong, E., Anderson, J.S., Zielinski, B.A., Fletcher, P.T., 2018. Riemannian Regression and Classification Models of Brain Networks Applied to Autism, in: *International Workshop on Connectomics in Neuroimaging*, Springer. pp. 78–87.

- Xie, Y., Vemuri, B.C., Ho, J., 2010. Statistical Analysis of Tensor Fields, in: International Conference on Medical Image Computing and Computer-Assisted Intervention, Springer. pp. 682–689.
- Xu, N., Doerschuk, P.C., Keilholz, S.D., Spreng, R.N., 2021. Spatiotemporal functional interactivity among large-scale brain networks. *NeuroImage* 227, 117628.
- Xu, Y., Lindquist, M.A., 2015. Dynamic connectivity detection: an algorithm for determining functional connectivity change points in fMRI data. *Frontiers in Neuroscience* 9, 285.
- Yaesoubi, M., Adali, T., Calhoun, V.D., 2018. A window-less approach for capturing time-varying connectivity in fMRI data reveals the presence of states with variable rates of change. *Human Brain Mapping* 39, 1626–1636.
- Yaesoubi, M., Allen, E.A., Miller, R.L., Calhoun, V.D., 2015. Dynamic coherence analysis of resting fMRI data to jointly capture state-based phase, frequency, and time-domain information. *NeuroImage* 120, 133–142.
- Yamin, A., Dayan, M., Squarcina, L., Brambilla, P., Murino, V., Diwadkar, V., Sona, D., 2019. Comparison Of Brain Connectomes Using Geodesic Distance On Manifold: A Twins Study, in: 2019 IEEE 16th International Symposium on Biomedical Imaging (ISBI 2019), IEEE. pp. 1797–1800.
- Yeo, B.T., Krienen, F.M., Sepulcre, J., Sabuncu, M.R., Lashkari, D., Hollinshead, M., Roffman, J.L., Smoller, J.W., Zöllei, L., Polimeni, J.R., et al., 2011. The organization of the human cerebral cortex estimated by intrinsic functional connectivity. *Journal of Neurophysiology* .
- You, K., Park, H.J., 2021. Re-visiting riemannian geometry of symmetric positive definite matrices for the analysis of functional connectivity. *NeuroImage* 225, 117464.

- Young, B.M., Nigogosyan, Z., Nair, V.A., Walton, L.M., Song, J., Tyler, M.E., Edwards, D.F., Caldera, K., Sattin, J.A., Williams, J.C., et al., 2014a. Case report: post-stroke interventional BCI rehabilitation in an individual with preexisting sensorineural disability. *Frontiers in Neuroengineering* 7, 18.
- Young, B.M., Nigogosyan, Z., Walton, L.M., Song, J., Nair, V.A., Grogan, S.W., Tyler, M.E., Edwards, D.F., Caldera, K., Sattin, J.A., et al., 2014b. Changes in functional brain organization and behavioral correlations after rehabilitative therapy using a brain-computer interface. *Frontiers in Neuroengineering* 7, 26.
- Zalesky, A., Breakspear, M., 2015. Towards a statistical test for functional connectivity dynamics. *NeuroImage* 114, 466–470.
- Zalesky, A., Fornito, A., Bullmore, E.T., 2010. Network-based statistic: identifying differences in brain networks. *NeuroImage* 53, 1197–1207.
- Zhang, J., Zhou, L., Wang, L., Li, W., 2015. Functional Brain Network Classification With Compact Representation of SICE Matrices. *IEEE Transactions on Biomedical Engineering* 62, 1623–1634.
- Zhang, L., Zuo, X.N., Ng, K.K., Chong, J.S.X., Shim, H.Y., Ong, M.Q.W., Loke, Y.M., Choo, B.L., Chong, E.J.Y., Wong, Z.X., et al., 2020. Distinct BOLD variability changes in the default mode and salience networks in Alzheimer’s disease spectrum and associations with cognitive decline. *Scientific Reports* 10, 1–12.
- Zhang, Z., Lu, G., Zhong, Y., Tan, Q., Chen, H., Liao, W., Tian, L., Li, Z., Shi, J., Liu, Y., 2010a. fMRI study of mesial temporal lobe epilepsy using amplitude of low-frequency fluctuation analysis. *Human Brain Mapping* 31, 1851–1861.
- Zhang, Z., Lu, G., Zhong, Y., Tan, Q., Liao, W., Wang, Z., Wang, Z., Li, K., Chen, H., Liu,

- Y., 2010b. Altered spontaneous neuronal activity of the default-mode network in mesial temporal lobe epilepsy. *Brain Research* 1323, 152–160.
- Zhao, Q., Kwon, D., Pohl, K.M., 2018. A Riemannian Framework for Longitudinal Analysis of Resting-State Functional Connectivity, in: *International Conference on Medical Image Computing and Computer-Assisted Intervention*, Springer. pp. 145–153.
- Zhao, Q., Sang, X., Metmer, H., Lu, J., Initiative, A.D.N., et al., 2019. Functional segregation of executive control network and frontoparietal network in Alzheimer’s disease. *Cortex* 120, 36–48.
- Zhi, D., Calhoun, V.D., Lv, L., Ma, X., Ke, Q., Fu, Z., Du, Y., Yang, Y., Yang, X., Pan, M., et al., 2018. Aberrant Dynamic Functional Network Connectivity and Graph Properties in Major Depressive Disorder. *Frontiers in Psychiatry* 9, 339.
- Zhou, Q., Zhang, L., Feng, J., Lo, C.Y.Z., 2019. Tracking the Main States of Dynamic Functional Connectivity in Resting State. *Frontiers in Neuroscience* 13, 685.
- Zhu, H., Huang, J., Deng, L., He, N., Cheng, L., Shu, P., Yan, F., Tong, S., Sun, J., Ling, H., 2019. Abnormal Dynamic Functional Connectivity Associated With Subcortical Networks in Parkinson’s Disease: A Temporal Variability Perspective. *Frontiers in Neuroscience* 13, 80.
- Zuo, X.N., Di Martino, A., Kelly, C., Shehzad, Z.E., Gee, D.G., Klein, D.F., Castellanos, F.X., Biswal, B.B., Milham, M.P., 2010. The Oscillating Brain: Complex and Reliable. *NeuroImage* 49, 1432–1445.